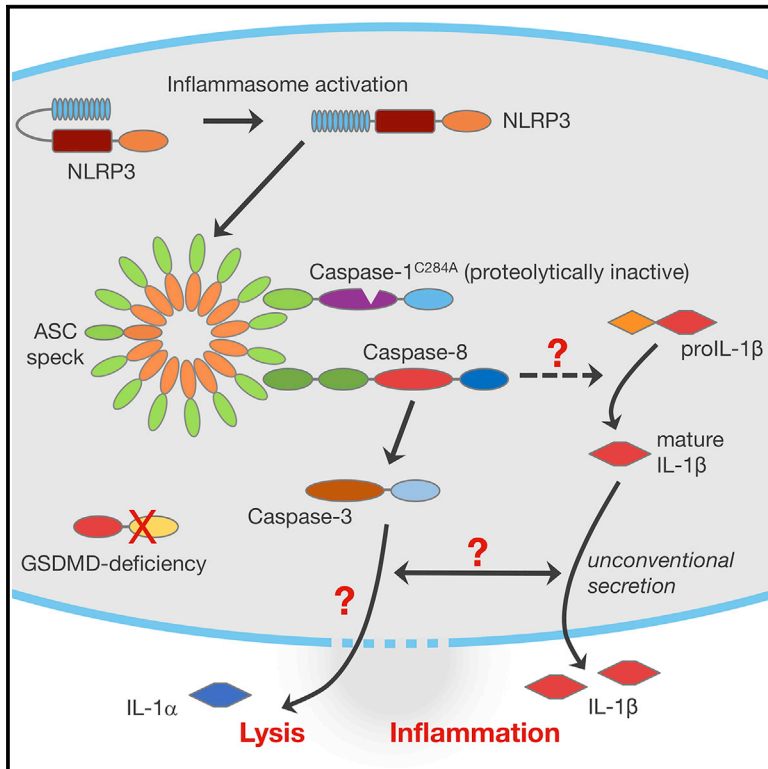


## The Inflammasome Drives GSDMD-Independent Secondary Pyroptosis and IL-1 Release in the Absence of Caspase-1 Protease Activity

### Graphical Abstract



### Authors

Katharina S. Schneider, Christina J. Groß, Roland F. Dreier, ..., Bernhard Kuster, Petr Broz, Olaf Groß

### Correspondence

olaf.gross@uniklinik-freiburg.de

### In Brief

Schneider et al. show that, in the absence of GSDMD or caspase-1 protease activity (e.g., in *Casp1<sup>C284A</sup>* mice), the inflammasome engages an alternative type of lytic cell death and IL-1 release that contributes to immunity against infection. This secondary form of pyroptosis is dependent on apoptotic caspase activity but distinct from apoptosis.

### Highlights

- Interplay of caspase-1 and caspase-8 revealed by analysis of *Caspase1<sup>C284A</sup>* mice
- GSDMD-dependent pyroptosis suppresses caspase-8 activation at the inflammasome
- The inflammasome engages caspase-8-driven secondary pyroptosis and IL-1 release
- GSDMD-independent mechanisms contribute to inflammasome-mediated host protection



# The Inflammasome Drives GSDMD-Independent Secondary Pyroptosis and IL-1 Release in the Absence of Caspase-1 Protease Activity

Katharina S. Schneider,<sup>1</sup> Christina J. Groß,<sup>1,2</sup> Roland F. Dreier,<sup>3</sup> Benedikt S. Saller,<sup>4</sup> Ritu Mishra,<sup>1,5</sup> Oliver Gorka,<sup>4</sup> Rosalie Heilig,<sup>3</sup> Etienne Meunier,<sup>3</sup> Mathias S. Dick,<sup>3</sup> Tamara Čiković,<sup>1,5</sup> Jan Sodenkamp,<sup>1,5,6</sup> Guillaume Médard,<sup>7</sup> Ronald Naumann,<sup>8</sup> Jürgen Ruland,<sup>1,5,6,9</sup> Bernhard Kuster,<sup>7,10</sup> Petr Broz,<sup>3,11</sup> and Olaf Groß<sup>1,2,4,5,12,\*</sup>

<sup>1</sup>Institute of Clinical Chemistry and Pathobiochemistry, Klinikum rechts der Isar, School of Medicine, Technical University of Munich, 81675 Munich, Germany

<sup>2</sup>BIOSS Centre for Biological Signaling Studies, University of Freiburg, 79104 Freiburg, Germany

<sup>3</sup>Focal Area Infection Biology, Biozentrum, University of Basel, 4056 Basel, Switzerland

<sup>4</sup>Institute of Neuropathology, Medical Center – University of Freiburg, Faculty of Medicine, University of Freiburg, 79106 Freiburg, Germany

<sup>5</sup>Center for Translational Cancer Research (TranslaTUM), Technical University of Munich, 81675 Munich, Germany

<sup>6</sup>German Cancer Consortium (DKTK), Partner Site Munich, 80336 Munich, Germany

<sup>7</sup>Chair of Proteomics and Bioanalytics, Technical University of Munich, 85354 Freising, Germany

<sup>8</sup>Max Planck Institute of Molecular Cell Biology and Genetics, 01307 Dresden, Germany

<sup>9</sup>German Center for Infection Research (DZIF), partner site Munich, 81675 Munich, Germany

<sup>10</sup>Center for Integrated Protein Science Munich (CIPSM), 81377 Munich, Germany

<sup>11</sup>Department of Biochemistry, University of Lausanne, 1066 Epalinges, Switzerland

<sup>12</sup>Lead Contact

\*Correspondence: [olaf.gross@uniklinik-freiburg.de](mailto:olaf.gross@uniklinik-freiburg.de)

<https://doi.org/10.1016/j.celrep.2017.12.018>

## SUMMARY

Inflammasomes activate the protease caspase-1, which cleaves interleukin-1 $\beta$  and interleukin-18 to generate the mature cytokines and controls their secretion and a form of inflammatory cell death called pyroptosis. By generating mice expressing enzymatically inactive caspase-1<sup>C284A</sup>, we provide genetic evidence that caspase-1 protease activity is required for canonical IL-1 secretion, pyroptosis, and inflammasome-mediated immunity. In caspase-1-deficient cells, caspase-8 can be activated at the inflammasome. Using mice either lacking the pyroptosis effector gasdermin D (GSDMD) or expressing caspase-1<sup>C284A</sup>, we found that GSDMD-dependent pyroptosis prevented caspase-8 activation at the inflammasome. In the absence of GSDMD-dependent pyroptosis, the inflammasome engaged a delayed, alternative form of lytic cell death that was accompanied by the release of large amounts of mature IL-1 and contributed to host protection. Features of this cell death modality distinguished it from apoptosis, suggesting it may represent a distinct form of pro-inflammatory regulated necrosis.

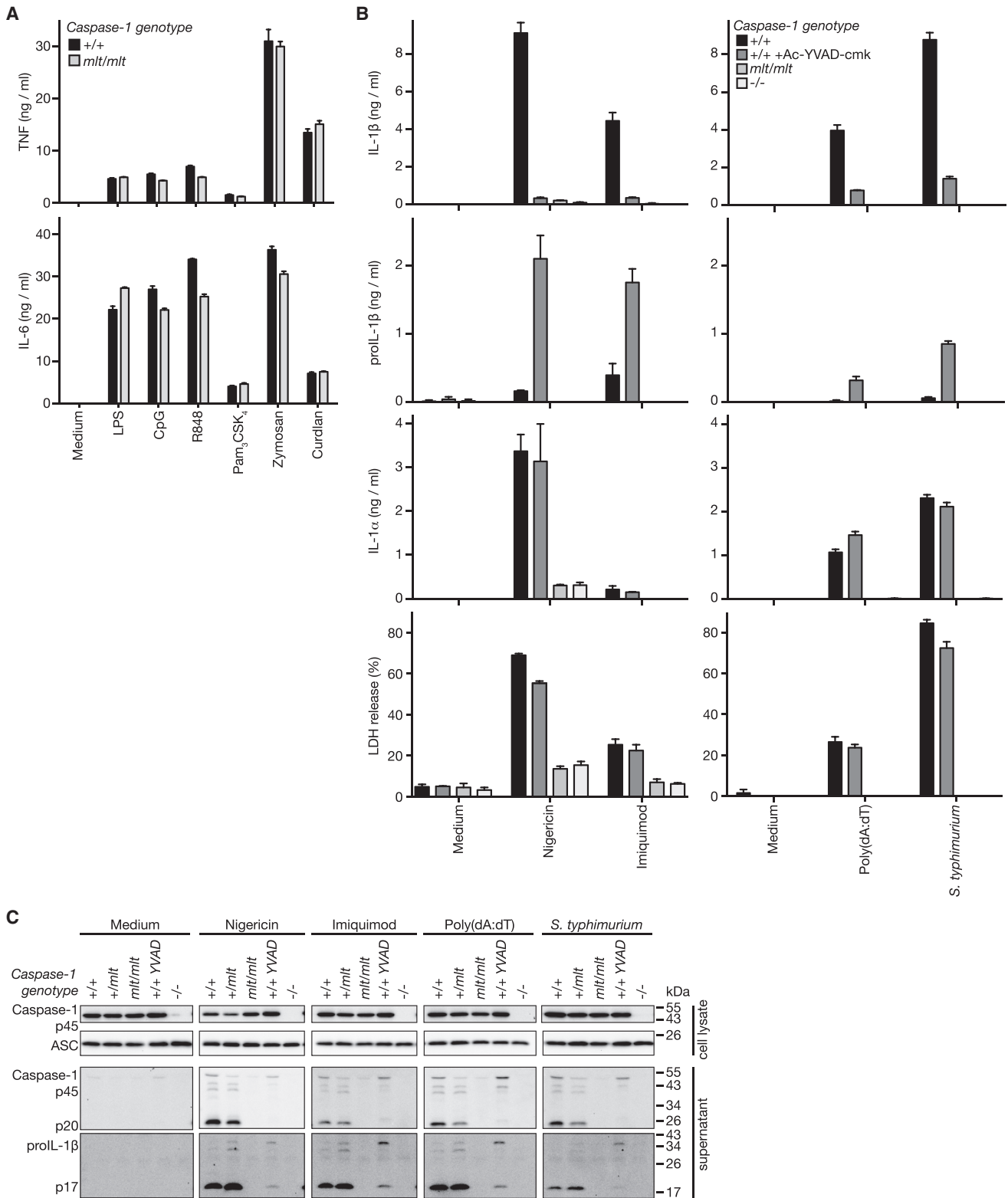
## INTRODUCTION

Caspases are cysteine aspartic proteases with essential roles in programmed cell death (Galluzzi et al., 2016). Previously known as interleukin-1 converting enzyme (ICE), caspase-1 is the prototypic inflammatory caspase (Kuida et al., 1995; Thornberry et al.,

1992). By promoting the activation of caspase-1, cytoplasmic complexes called inflammasomes control the proteolytic maturation of the pro-inflammatory cytokine interleukin (IL)-1 $\beta$ , which cannot bind the IL-1 receptor in its unprocessed form (Broz and Dixit, 2016). IL-1 $\beta$  lacks a signal peptide, so it cannot be secreted by the conventional pathway via the endoplasmic reticulum and Golgi apparatus. It instead leaves the cell by a poorly understood unconventional secretory pathway engaged by caspase-1. Inflammasome activation results in pyroptosis, a specialized form of lytic, inflammatory cell death defined by its dependence on inflammatory caspases (Galluzzi et al., 2016). Activation of caspase-11 (caspase-4 and caspase-5 in humans) by lipopolysaccharide (LPS) in the cytoplasm also results in pyroptosis (Kayagaki et al., 2011). By forming membrane pores, gasdermin D (GSDMD) executes cell death and IL-1 secretion initiated by inflammatory caspases (Ding et al., 2016; He et al., 2015; Kayagaki et al., 2015; Liu et al., 2016; Sborgi et al., 2016; Shi et al., 2015).

We previously observed that the secretion of IL-1 $\alpha$  by myeloid cells is caspase-1 dependent but insensitive to peptide-based inhibitors of caspase-1 (Groß et al., 2012). IL-1 $\alpha$  and IL-1 $\beta$  bind the same receptor (IL1R1), but in contrast to IL-1 $\beta$ , IL-1 $\alpha$  is not cleaved by caspase-1 and is active in its full-length form. In the presence of these inhibitors, cleavage of IL-1 $\beta$  is blocked, but IL-1 $\beta$  is secreted in its full-length form. Furthermore, when activated independent of ASC at the NLRC4 or NLRP1 inflammasomes, caspase-1 can induce pyroptosis without processing IL-1 $\beta$  or itself. Peptide-based inhibitors are unable to block this cell death (Broz et al., 2010). Altogether, these results suggested that caspase-1 may have a non-enzymatic or scaffold function that controls secretion of IL-1 and pyroptosis. In support of this concept, pro-inflammatory functions that do not strictly rely on enzymatic activity have also been ascribed to caspase-8 (Kang et al., 2015; Lemmers et al., 2007; Philip et al., 2016; Su et al., 2005) and the paracaspase





MALT1 (Gewies et al., 2014). Furthermore, several mutations in the *CASP1* gene that suppress caspase-1 protease activity have been found in patients with auto-inflammatory conditions that resemble periodic fever syndromes associated with mutations in *NLRP3* or other inflammasome genes (Luksch et al., 2013).

These indications that caspase-1 may have a pro-inflammatory function independent of its enzymatic activity prompted us to generate mice deficient for caspase-1 protease activity. With these *Casp1<sup>mit</sup>* (melted) mice, we demonstrate that in contrast to biochemical inhibition, genetic inactivation of caspase-1 protease activity impairs not only cleavage of IL-1 $\beta$  but also canonical IL-1 secretion and pyroptosis at early time points. Caspase-8 is recruited to the inflammasome and, in caspase-1-deficient cells, drives late, non-canonical maturation of IL-1 $\beta$  (Antonopoulos et al., 2015; Pierini et al., 2013). This phenomenon was also observed in cells expressing enzymatically inactive caspase-1<sup>mit</sup>. Caspase-8 activation at inflammasomes was suppressed by GSDMD-dependent pyroptosis, rather than caspase-1 protease activity per se. Despite efficient caspase-1-mediated maturation of IL-1 $\beta$  in GSDMD-deficient cells, the rapid, canonical secretion of IL-1 $\beta$  was impaired. However, in the absence of GSDMD-dependent pyroptosis, cells engaged a delayed non-canonical release mechanism that, despite apoptotic caspase activation, was distinct from apoptosis and over time allowed for secretion of equivalent amounts of IL-1 $\beta$ .

## RESULTS

### Generation and Characterization of *Casp1<sup>mit</sup>* Mice

An active site cysteine participates in the proteolytic mechanism of caspases, including caspase-1 (Thornberry et al., 1992). To generate mice lacking caspase-1 protease activity, targeting vectors for the introduction of the inactivating C284A mutation into exon 6 of the murine *Casp1* genomic locus were cloned (Figures S1A and S1B). The mutation changes the genomic sequence from 5'-GCATGCCGT-3' to 5'-GCAGCGCGT-3', which translates into the amino acid sequence AAR instead of ACR. The mutation also generated a HhaI restriction site (GCG $\cdot$ C) that was used for screening and genotyping (Figure S1C).

Bone marrow-derived dendritic cells (BMDCs) from mice homozygous for the *Casp1<sup>mit</sup>* mutation expressed caspase-1 protein at normal levels (Figure S1D). Interbreeding of heterozygous mice produced offspring in the expected Mendelian ratios. Mice homozygous for the *Casp1<sup>mit</sup>* mutation had growth curves and fertility indistinguishable from their wild-type littermates (Figures S1E–S1H). Immunophenotyping analysis was performed on lymphoid organs of 8-week-old *Casp1<sup>mit/mit</sup>* mice and wild-type littermates. *Casp1<sup>mit/mit</sup>* mice and wild-type mice had indistinguishable numbers and frequencies of the major immune cell subsets (Figure S1I; data not shown). Patients with mutations in *CASP1* resulting in impaired protease activity display auto-inflammation

(Luksch et al., 2013). However, under specific pathogen-free (SPF) and specific and opportunistic pathogen-free (SOPF) conditions, mice homozygous for the *Casp1<sup>mit</sup>* mutation were healthy and did not show obvious signs of spontaneous inflammation or immunosuppression.

### Caspase-1 Protease Activity Is Required for Canonical IL-1 Secretion, Pyroptosis, and Innate Immunity to *Francisella*

BMDCs from *Casp1<sup>mit/mit</sup>* mice secreted comparable amounts of tumor necrosis factor (TNF) and IL-6 upon engagement of various Toll-like receptors and C-type lectin receptors and did not spontaneously secrete these cytokines (Figure 1A). To genetically test whether caspase-1 protease activity is required for IL-1 secretion and pyroptosis, BMDCs from *Casp1<sup>mit/mit</sup>*, *Casp1<sup>-/-</sup>*, and wild-type mice were primed with LPS and then treated for up to 3 hr with activators of the NLRP3 (nigericin and imiquimod), AIM2 (poly(dA:dT)), and NLRC4 (*Salmonella enterica* serovar Typhimurium [*S. typhimurium*]) inflammasomes. Mature IL-1 $\beta$ , pro-IL-1 $\beta$ , and IL-1 $\alpha$  were quantified in the supernatants by ELISA (Figure 1B), and cell lysates and supernatants were analyzed by immunoblotting (Figure 1C) for the presence of the cleaved and full-length forms of IL-1 $\beta$  and caspase-1. Lactate dehydrogenase (LDH) activity was measured from supernatants as a readout for pyroptosis (Figure 1B). Inflammasome activators induced the secretion of cleaved caspase-1 and IL-1 $\beta$  from cells expressing wild-type caspase-1. Similar to *Casp1<sup>-/-</sup>* cells, *Casp1<sup>mit/mit</sup>* cells not only failed to cleave IL-1 $\beta$  but also did not secrete pro-IL-1 $\beta$  or IL-1 $\alpha$  and did not undergo pyroptosis at time points up to 3 hr (Figure 1B). As previously observed (Broz et al., 2010; Grob et al., 2012), the peptide-based caspase-1 inhibitor Ac-YVAD-cmk strongly reduced cleavage of IL-1 $\beta$  and caspase-1, but cells treated with this inhibitor still secreted the uncleaved forms of these proteins and underwent pyroptosis (Figures 1B and 1C). This demonstrates that caspase-1 protease activity is required for early, canonical IL-1 secretion and pyroptosis and suggests that peptide-based caspase-1 inhibitors fail to prevent these outcomes of caspase-1 activity.

We targeted the caspase-1 allele in both 129 and C57BL/6 embryonic stem cells (Figures S1A and S1B). Gene targeting is known to be more efficient in 129 embryonic stem cells, but inactivating mutations in the *Casp11* gene of this strain cannot be segregated from introduced mutations in *Casp1* (Kayagaki et al., 2011). Because B6.129-*Casp1<sup>mit</sup>* mice were generated several months before B6-*Casp1<sup>mit</sup>* mice, and because the appropriate controls (the original B6.129-*Casp1<sup>-/-</sup>* [*ICE<sup>-/-</sup>*] mice that harbor the inactivating *Casp11* mutation) were readily available (Kuida et al., 1995), the *in vitro* studies were first performed in B6.129-*Casp1<sup>mit</sup>* mice (Figure 1) and then confirmed in B6-*Casp1<sup>mit</sup>* mice (Figures S2A–S2C). We also generated B6-*Casp1<sup>-/-</sup>* mice using CRISPR/Cas9 technology to use as

(B) BMDCs from the indicated mouse strains (B6.129-*Casp1<sup>mit/mit</sup>* and B6.129-*Casp11/11<sup>-/-</sup>*) were primed with LPS (50 ng/mL for 3 hr) and subsequently stimulated with agents activating the NLRP3 (nigericin and imiquimod), AIM2 (poly(dA:dT)), and NLRC4 (*Salmonella enterica* serovar Typhimurium) inflammasomes. IL-1 $\beta$ , pro-IL-1 $\beta$ , and IL-1 $\alpha$  (top) and LDH (bottom) were quantified from cell-free supernatants by ELISA and a colorimetric assay, respectively. (C) Cleavage and secretion of caspase-1 and IL-1 $\beta$  in BMDCs following inflammasome activation as in (B) were determined by immunoblotting (B6.129-*Casp1<sup>mit/mit</sup>*).

In (A) and (B), mean  $\pm$  SEM are shown. In (B and C), data are representative of >10 independent experiments.

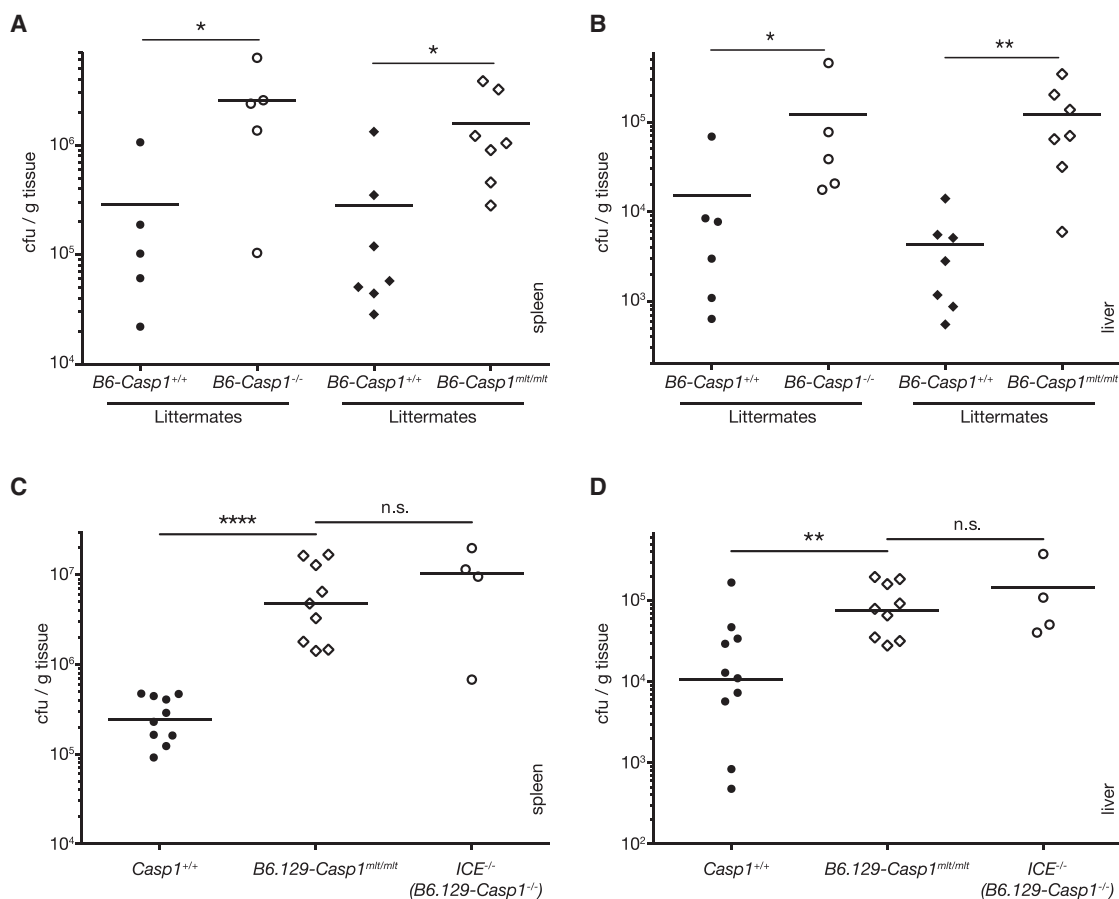


**Figure 2. Caspase-1 Protease Activity Is Required for Innate Immunity to *Francisella***

(A–D) Bacterial loads in spleens (A and C) and livers (B and D) of mice infected with *Francisella novicida* for 48 hr were determined by plating serial dilutions of organ homogenates on selective medium plates. In (C) and (D), the wild-type group consists of littermates of B6.129-Casp1<sup>mt/mt</sup> mice; B6.129-Casp1<sup>-/-</sup> animals were matched by age and sex and were bred in the same isolator. The Mann-Whitney test was used for statistical analysis (\*p < 0.05, \*\*p < 0.01, \*\*\*p < 0.001, \*\*\*\*p < 0.0001). (A and B) Spleen: Casp1<sup>-/-</sup>, p = 0.0317; Casp1<sup>mt/mt</sup>, p = 0.0175; liver: Casp1<sup>-/-</sup>, p = 0.0303; Casp1<sup>mt/mt</sup>, p = 0.00012; B6-Casp1<sup>-/-</sup> and littermate B6-Casp1<sup>+/+</sup>; n = 5; B6-Casp1<sup>mt/mt</sup> and littermate B6-Casp1<sup>+/+</sup>; n = 7. (C and D) Spleen: Casp1<sup>mt/mt</sup>, p < 0.0001; liver: Casp1<sup>mt/mt</sup>, p = 0.0076; B6.129-Casp1<sup>mt/mt</sup> and littermate B6.129-Casp1<sup>+/+</sup>; n = 9 and n = 10, respectively; B6.129-Casp1<sup>-/-</sup>; n = 4.

controls for B6-Casp1<sup>mt</sup> mice. Previous studies have established a requirement for caspase-1 activation via the DNA-sensing AIM2 inflammasome for innate immunity against the facultative intracellular pathogen *Francisella tularensis* subspecies *novicida* (*F. novicida*) (Fernandes-Alnemri et al., 2010). Similar to Casp1<sup>-/-</sup> mice, Casp1<sup>mt/mt</sup> mice from both the C57BL/6 and the 129 backgrounds were susceptible to *Francisella*, displaying an elevated bacterial load in the spleen and liver upon infection (Figure 2). These results demonstrate that caspase-1 protease activity is required for protection against *Francisella*.

### Caspase Inhibitors Vary in Their Ability to Prevent GSDMD Cleavage and Pyroptosis

Because genetic inactivation of caspase-1 protease activity prevented both IL-1 secretion and pyroptosis at early time points, we examined why peptide-based inhibitors of caspase-1 have a qualitatively different effect. The effect of VX-765, a new pep-

tidomimetic inhibitor of caspase-1 (Wannamaker et al., 2007), on secretion of cleaved IL-1 $\beta$  was comparable to that of Ac-YVAD-cmk (Figure 3A). In contrast to Ac-YVAD-cmk, VX-765 prevented pyroptosis (Figure 3A). GSDMD was identified as a cleavage target of caspase-1 and caspase-11 (Agard et al., 2010) required for pyroptosis and IL-1 secretion (He et al., 2015; Kayagaki et al., 2015; Shi et al., 2015). The differential ability of VX-765 and Ac-YVAD-cmk to inhibit pyroptosis was reflected in the prevention of GSDMD cleavage by VX-765, but not by Ac-YVAD-cmk (Figure 3B). The pan-caspase inhibitor Z-VAD-fmk prevented GSDMD cleavage only at toxic concentrations in which it alone caused release of cytoplasmic proteins, presumably by inducing necroptosis (Figures 3B and S3). Consistent with the inability of Casp1<sup>mt/mt</sup> cells to pyroptose at early time points, GSDMD cleavage was not observed in Casp1<sup>mt/mt</sup> cells after treatment with inflammasome activators (Figure 3C). The release of the uncleaved pro-form of IL-1 $\beta$  in the presence of caspase-1 inhibitors at early time points was

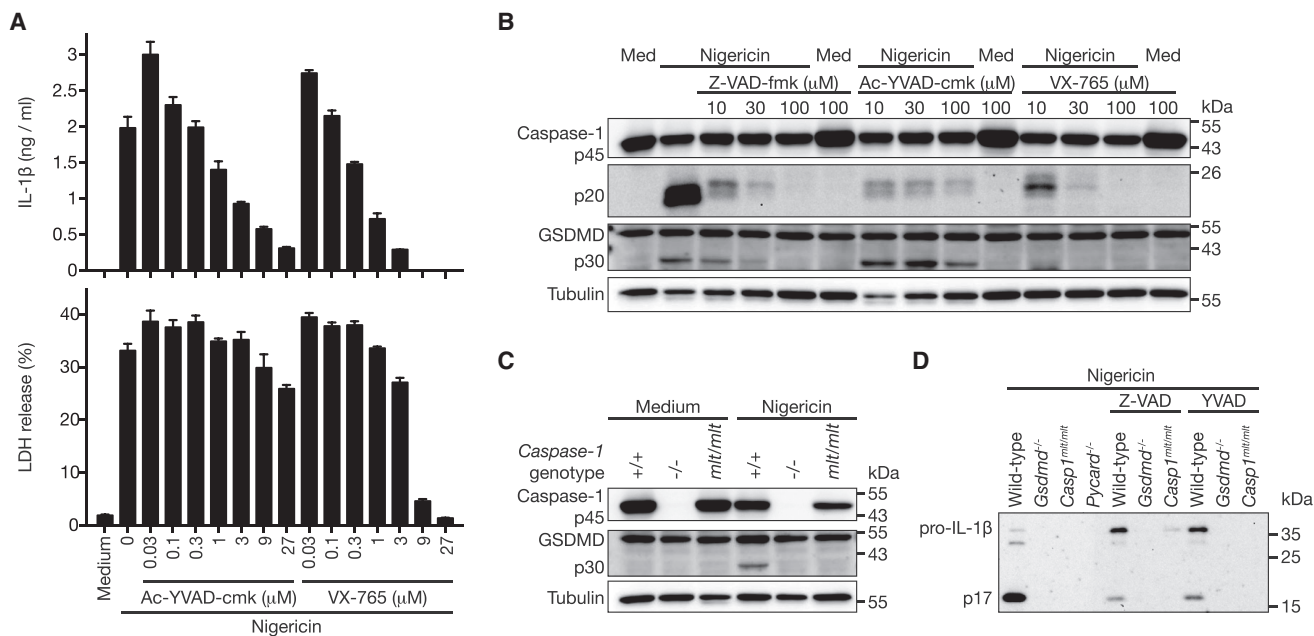


**Figure 3. Caspase Inhibitors Vary in Their Ability to Prevent GSDMD Cleavage and Pyroptosis**

(A) BMDCs were pretreated with the indicated doses of the caspase-1 inhibitors Ac-YVAD-cmk and VX-765 for 30 min and stimulated with 5 μM nigericin for 45 min, and secretion of IL-1β and release of LDH into the supernatant were measured (mean ± SEM are shown).

(B) BMDCs were pretreated with caspase inhibitors as indicated and stimulated with nigericin. Caspase-1 and GSDMD cleavage were assessed by immunoblot analysis.

(C) BMDCs from wild-type, B6.129-Casp1<sup>-/-</sup>, and B6.129-Casp1<sup>mit/mit</sup> mice were stimulated with nigericin, and GSDMD cleavage was analyzed in cytoplasmic fractions by immunoblotting.

(D) BMDCs from the indicated mouse strains (B6.129-Casp1<sup>mit/mit</sup>) were pretreated with caspase inhibitor Z-VAD-fmk (20 μM) or Ac-YVAD-cmk (30 μM) and stimulated with nigericin for 1.5 hr. Secretion of the cleaved and uncleaved forms of IL-1β was assessed by immunoblot analysis from cell-free cell culture supernatants.

(A–C) Data representative of ≥ 3 independent experiments.

GSDMD dependent (Figure 3D). Altogether, these results suggest that VX-765 is a superior caspase-1 inhibitor and that residual cleavage of GSDMD in the presence of Ac-YVAD-cmk is sufficient for pyroptosis and IL-1 release.

### Caspase-1<sup>mit</sup> Accumulates at the Inflammasome

A common feature of inflammasome activation is ASC polymerization and formation of a detergent-insoluble speck (Fernandes-Alnemri et al., 2007). To determine whether protease activity of caspase-1 influences its ability to be recruited to the ASC speck, wild-type and Casp1<sup>mit/mit</sup> BMDCs were treated with inflammasome activators, and inflammasome formation was monitored by confocal and super-resolution immunofluorescence microscopy of fixed cells and immunoblotting of the detergent-insoluble fraction of cells. Caspase-1<sup>mit</sup> strongly accumulated at the inflammasome or speck (Figures 4A–4C and S4A), presumably because unlike wild-type caspase-1, it fails to liberate itself by auto-cleavage. Treatment with the caspase-1 inhibitor Ac-YVAD-cmk also caused caspase-1 to accumulate at the inflammasome (Figure 4A).

Our results suggested that caspase-1 protease activity is critical for canonical IL-1 secretion and pyroptosis but do not rule out that caspase-1 may have functions that do not strictly require protease activity. The accumulation of caspase-1<sup>mit</sup> in the insoluble fraction

presented a means to enrich factors that stably interact with caspase-1 at the inflammasome yet avoid potential confounding effects of pyroptosis. Cells of genotypes incapable of caspase-1-dependent pyroptosis were treated with nigericin, and the insoluble fraction (Figure 4C) was prepared in quadruplicate and analyzed by label-free mass spectrometry. As expected, ASC was consistently enriched in the insoluble fraction of Casp1<sup>mit/mit</sup> cells relative to Nlrp3<sup>-/-</sup> cells (Figure 4D). Caspase-1 was also strongly enriched in the insoluble fraction of Casp1<sup>mit</sup> cells relative to Nlrp3<sup>-/-</sup> and Casp1<sup>-/-</sup> cells. However, more than 1,000 other proteins were detected in this cellular fraction, and none of them were reproducibly enriched in an NLRP3- or caspase-1-dependent manner. The strong enrichment of caspase-1 and ASC in this fraction indicates that they are the most abundant components of the inflammasome, but it is clear that better purification techniques will be required to identify potential regulatory components with lower abundance. For example, while caspase-8 can be found in ASC specks (Figures 5A and 5B) (Sagulenko et al., 2013), it was not detected by mass spectrometry.

### Enhanced Activation of Caspase-8 and Non-canonical IL-1β Processing in Cells Expressing Caspase-1<sup>mit</sup>

Although ASC-containing inflammasomes can recruit caspase-8, the initiator caspase of the extrinsic apoptosis pathway,

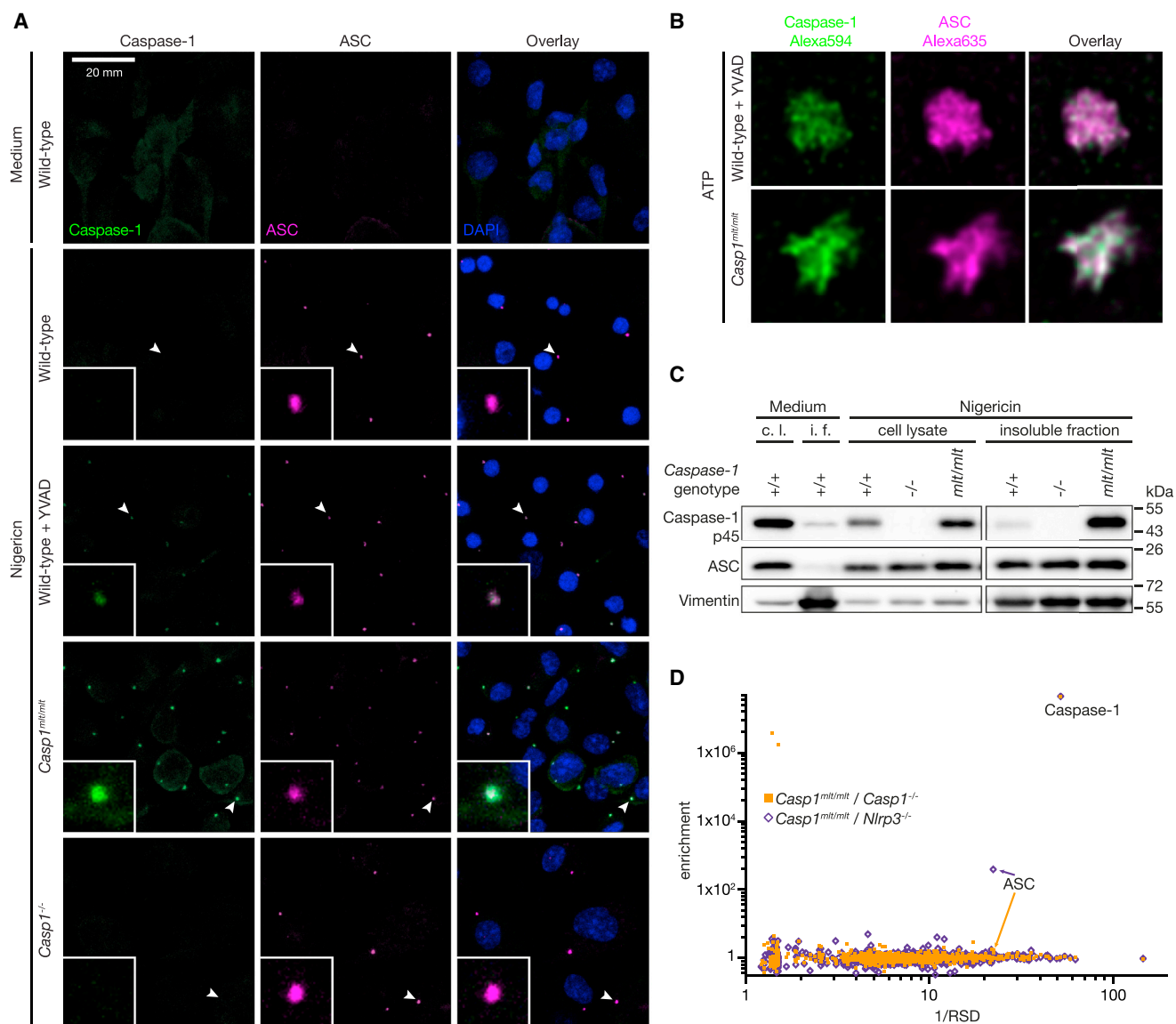


**Figure 4. Caspase-1<sup>mit</sup> Accumulates at the Inflammasome**

(A) BMDCs from B6.129-*Casp1<sup>mit/mit</sup>* or wild-type mice on culture slides were pretreated with 20  $\mu$ M Ac-YVAD-cmk where indicated and subsequently stimulated with nigericin. Cells were fixed with paraformaldehyde, stained by immunofluorescence for caspase-1 (green) and ASC (magenta), and analyzed by confocal microscopy. DAPI (blue) localizes with the nuclei. Scale bar represents 20  $\mu$ m (data representative of >5 independent experiments).

(B) BMDCs from B6.129-*Casp1<sup>mit/mit</sup>* or wild-type mice on culture slides, the latter pretreated with 20  $\mu$ M Ac-YVAD-cmk, were stimulated with nigericin, fixed, and stained by immunofluorescence for caspase-1 (green) and ASC (magenta). ASC specks were visualized at high resolution by STED imaging.

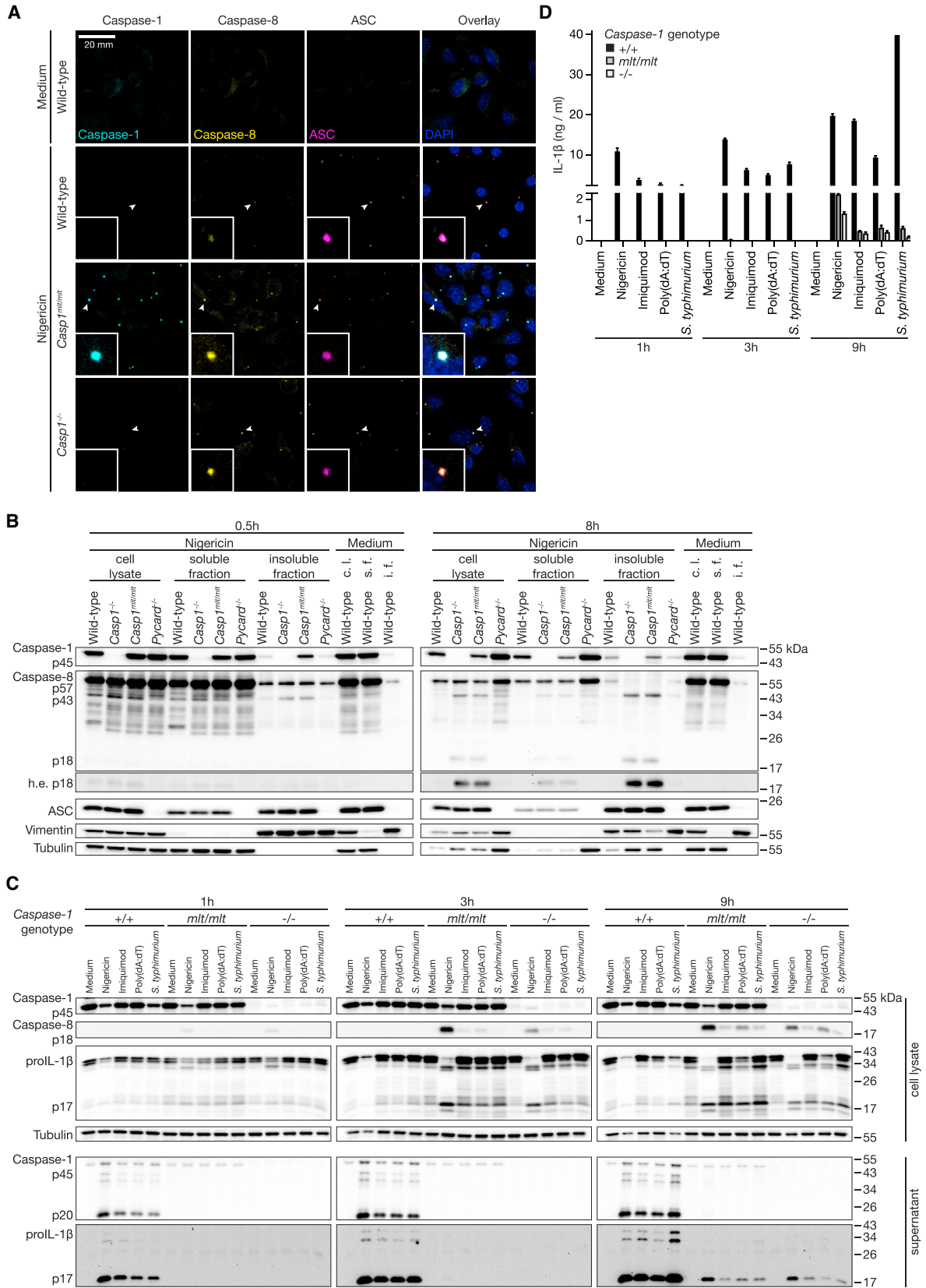
(C) BMDCs of the indicated genotypes (B6.129-*Casp1<sup>-/-</sup>* and B6.129-*Casp1<sup>mit/mit</sup>*) were primed with LPS and subsequently stimulated with nigericin. An IGEPAL CA-630-insoluble fraction was isolated by centrifugation, and cell lysates, insoluble fractions, and soluble fractions were analyzed for the presence of ASC, caspase-1, and vimentin as fractionation control by immunoblotting. c.l., cell lysate; i.f., insoluble fraction.

(D) Four replicates each of BMDCs from B6.129-*Casp1<sup>mit/mit</sup>*, *Nlrp3<sup>-/-</sup>*, and B6.129-*Casp1<sup>-/-</sup>* were stimulated and prepared as in (C), and insoluble fraction samples were analyzed by mass spectrometry. The relative enrichment of proteins detected in B6.129-*Casp1<sup>mit/mit</sup>* over *Nlrp3<sup>-/-</sup>* or B6.129-*Casp1<sup>-/-</sup>* samples is plotted against the inverse relative SD (RSD) within the B6.129-*Casp1<sup>mit/mit</sup>* quadruplet (mean/SD).

(C and D) Data representative of 2 independent experiments with n = 4 replicates per genotype.

pyroptosis is the predominant form of cell death in response to inflammasome activators when caspase-1 is present. However, in the absence of caspase-1, caspase-8 is activated at the inflammasome and has been reported to be associated with features of apoptosis (Antonopoulos et al., 2015; Pierini et al.,

2012; Sagulenko et al., 2013). One possible explanation for the activation of caspase-8 is that in the absence of caspase-1, naked ASC specks can more efficiently recruit caspase-8. However, recruitment of caspase-8 to ASC specks was similar in *Casp1<sup>mit/mit</sup>* cells and *Casp1<sup>-/-</sup>* cells (Figures 5A, S4B, and



(legend on next page)

S4C). This also suggests that caspase-1 and caspase-8 do not compete for the same binding sites at the inflammasome. Consistent with this idea and previous biochemical and structural studies (Fu et al., 2016; Vajjhala et al., 2015), caspase-1 and caspase-8 occupied distinct areas in inflammasomes imaged by super-resolution microscopy (Figure S4D). Although most ASC specks in all genotypes displayed some caspase-8 positivity, caspase-8 recruitment was markedly enhanced in the absence of caspase-1 activity (Figures 5A, S4B, and S4C). However, immunoblotting analysis revealed that only a small fraction of the cellular pool of caspase-8 was recruited to the inflammasome (Figure 5B). This is consistent with previous observations (Sagulenko et al., 2013) and could explain why we did not detect caspase-8 by mass spectrometry. Similarly, the caspase-8 interaction partners cFLIP, FADD, and RIPK1 were also detected in the specks, together with caspase-8, when caspase-1 was absent (Figures S5A and S5B).

Cleavage of caspase-8 to generate the active p18 fragment was also similar between *Casp1*<sup>-/-</sup> and *Casp1*<sup>mtl/mtl</sup> cells (Figures 5B and 5C). This phenomenon required formation of the inflammasome platform, because cleavage of caspase-8 was not observed in the absence of ASC (*Pycard*<sup>-/-</sup>) (Figure 5B), as reported previously (Antonopoulos et al., 2015; Pierini et al., 2012; Sagulenko et al., 2013). Caspase-8 cleavage was readily detected in *Casp1*<sup>-/-</sup> and *Casp1*<sup>mtl/mtl</sup> cells after 3 hr of inflammasome activation but could also be observed as early as 1 hr after stimulation with nigericin (Figure 5C). Although caspase-8 is recruited to the ASC speck in wild-type cells (Figures 5A, S4B, and S4C), cleavage of caspase-8 was not observed in wild-type cells treated with several inflammasome activators for up to 24 hr (Figure S5C).

Caspase-8 can directly cleave IL-1 $\beta$  to generate the mature form (Maelfait et al., 2008), and caspase-8 activation at the ASC speck in caspase-1-deficient cells can lead to non-canonical (caspase-1-independent) IL-1 $\beta$  maturation after prolonged activation of the inflammasome (Antonopoulos et al., 2013; Pierini et al., 2013). Wild-type cells rapidly secreted cleaved IL-1 $\beta$  as expected (Figures 5C and 5D). The non-canonical cleavage of IL-1 $\beta$  in *Casp1*<sup>-/-</sup> and *Casp1*<sup>mtl/mtl</sup> cells correlated with activation of caspase-8 and was inhibited by the pan-caspase inhibitor Z-VAD-fmk and the caspase-8 inhibitor IETD-fmk (Figures 5C, 5D, and S5D). *Casp1*<sup>-/-</sup> and *Casp1*<sup>mtl/mtl</sup> cells, but not ASC-deficient cells (Figure S5C), also secreted mature IL-1 $\beta$  after prolonged stimulation with inflammasome activators, which suggests that these cells engage a non-canonical but ASC-dependent secretion pathway that does not rely on caspase-1

protease activity (Figures 5D and S5C). However, wild-type cells secreted substantially more IL-1 $\beta$  than did *Casp1*<sup>-/-</sup> and *Casp1*<sup>mtl/mtl</sup> cells (Figures 5C and 5D), indicating that the efficiency of either IL-1 $\beta$  processing or IL-1 $\beta$  release is reduced in the absence of caspase-1 activity.

### Inflammasome-Induced Lytic Cell Death and IL-1 Release in GSDMD-Deficient Cells

Our data suggest that enhanced inflammasome-induced caspase-8 activation in the absence of caspase-1 was not merely a consequence of increased availability of potential binding sites on ASC and instead implied that the absence of caspase-1 protease activity or a consequence thereof permits caspase-8 activation at the inflammasome. Thus, we asked how caspase-1 protease activity suppresses caspase-8 activation at the inflammasome. Aside from itself, IL-1 $\beta$ , and GSDMD, caspase-1 has several other substrates that could potentially account for this phenomenon (Agard et al., 2010; Denes et al., 2012). As expected, short-term ( $\leq 3$  hr) stimulation with inflammasome activators triggered release of cleaved IL-1 $\beta$  and LDH from wild-type cells, but not from cells lacking GSDMD, caspase-1, or caspase-1 protease activity (Figures 6A and 6B). Similar to *Casp1*<sup>-/-</sup> and *Casp1*<sup>mtl/mtl</sup> cells and in contrast to wild-type cells, GSDMD-deficient cells displayed robust caspase-8 activation (Figure 6A). This indicates that caspase-1 activity results in the suppression of caspase-8 activation by inducing GSDMD-dependent pyroptosis. Gradual loss of intracellular caspase-8 was observed during GSDMD-dependent pyroptosis, and it is possible that this contributes to the reduced activation of caspase-8 in wild-type cells (Figures 5B and S5D). However, inhibition of pyroptotic lysis in wild-type cells by addition of glycine (Brennan and Cookson, 2000) did not restore caspase-8 activation (Figures S5D and S5E), suggesting that lysis is not the primary reason for suppression of inflammasome-induced caspase-8 activity in wild-type cells. Both caspase-1 and caspase-8 are activated in GSDMD-deficient cells, and this coincided with stronger intracellular cleavage of IL-1 $\beta$  (generating the bioactive p17 subunit) than was observed in cells lacking caspase-1 protease activity. Other caspase-dependent (Figure S5D) IL-1 $\beta$  cleavage and degradation products were observed in cells lacking caspase-1 protease activity, but these were not released (Figures 5C and 6A). IL-1 $\beta$  p17 was initially retained in cells; its delayed but robust GSDMD-independent release coincided with release of the lytic cell death marker LDH (Figures 6A and 6B) and the alarmin IL-1 $\alpha$  (Figure S6A). The late LDH release was comparable in GSDMD-deficient cells, in which both caspase-1 and caspase-8 are

### Figure 5. Enhanced Activation of Caspase-8 in Cells Expressing Caspase-1<sup>mtl</sup>

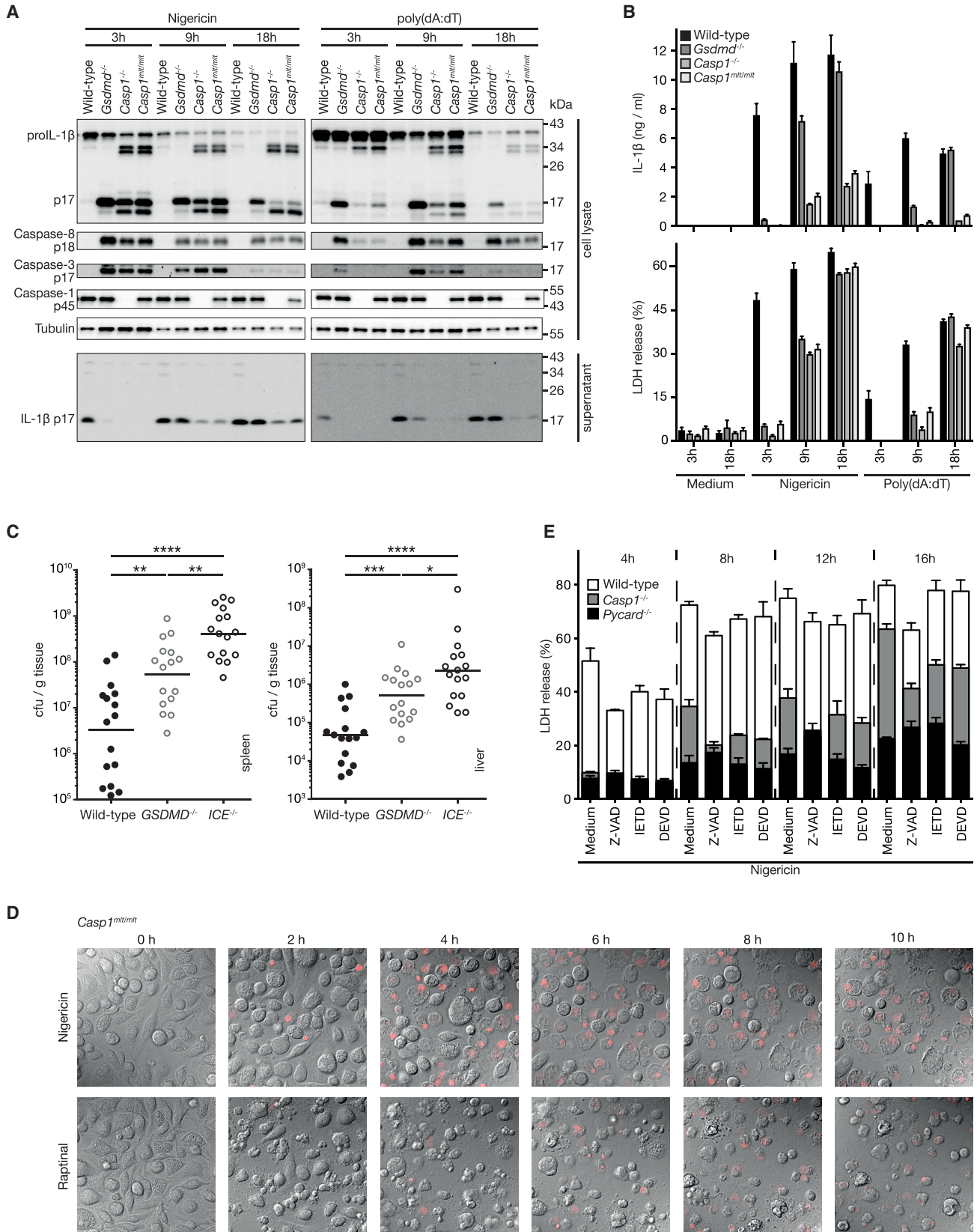
(A) BMDCs of the indicated genotypes (B6.129-*Casp1*<sup>mtl/mtl</sup>) on culture slides were stimulated with nigericin, fixed, and stained by immunofluorescence for caspase-1 (cyan), caspase-8 (yellow), and ASC (magenta), and then confocal imaging was performed. DAPI (blue) localizes with the nuclei. Scale bar represents 20  $\mu$ m (data representative of >5 independent experiments).

(B) BMDCs from different *Casp1* genotypes as indicated (B6-*Casp1*<sup>mtl/mtl</sup>) and ASC-deficient cells (*Pycard*<sup>-/-</sup>) were investigated for recruitment of caspase-8 into IGEPAAL CA-630-insoluble fractions following LPS priming and inflammasome activation by nigericin (for 0.5 or 8 hr) (data representative of 2 independent experiments). c.l., cell lysate; s.f., soluble fraction; i.f., insoluble fraction; h.e., high exposure.

(C) Cleavage and secretion of IL-1 $\beta$  and caspase-1 and generation of caspase-8 p18 were monitored by immunoblot analysis 1, 3, and 9 hr after stimulation of BMDCs from the indicated genotypes (B6-*Casp1*<sup>mtl/mtl</sup>) with nigericin, imiquimod (70  $\mu$ M), poly(dA:dT) (1  $\mu$ g/mL), and *Salmonella enterica* serovar Typhimurium (MOI 20).

(D) Secretion of mature IL-1 $\beta$  in conditions as in (C) was measured by ELISA (mean  $\pm$  SEM are shown).

In (C) and (D), data are representative of 5 independent experiments.



(legend on next page)

**Table 1. Summary of the Molecular and Cellular Features of Secondary Pyroptosis in Comparison to Other Forms of Cell Death**

	Apoptosis	Necroptosis	Pyroptosis	Secondary Pyroptosis	Source
ASC dependent	–	–	+	+	1, 2, 3, this manuscript
Caspase-1 dependent	–	–	+	–	1, 2, 3, this manuscript
GSDMD dependent	–	–	+	–	This manuscript
Cell swelling	–	+	+	+	This manuscript
Blebbing, formation of apoptotic bodies	+	–	–	–	This manuscript
Loss of membrane integrity (i.e., propidium iodide, DRAQ7 uptake)	–	+	+	+	1, 2, 3, this manuscript
Cell lysis, LDH release	–	+	+	+	1, 3, this manuscript
Phosphatidylserine exposure	++	+	+	+	1, this manuscript
Pore formation	–	+ MLKL	+ GSDMD	ND <sup>a</sup>	ND
Caspase-8 activation	+	–	–	+	1, 2, 3, this manuscript
Caspase-3 activation	+	–	–	+	1, 2, 3, this manuscript
PARP cleavage	++	–	+	++	This manuscript
DNA fragmentation	+	+	–(+) <sup>b</sup>	+	1, 2
Nuclear condensation	+	+	+	+	1, this manuscript
NEC1 sensitivity	–	+	–	–	This manuscript
Sensitive to caspase inhibitors	+++	(–) <sup>c</sup>	±	+	This manuscript
IL-1 release	–	–	++	++	3, this manuscript

The source column refers to the description of cell death induced by the inflammasome but independent of caspase-1. Previous reports characterized this cell death as apoptosis: (1) Pierini et al. (2012), (2) Sagulenko et al. (2013), and (3) Antonopoulos et al. (2015).

<sup>a</sup>The effector of secondary pyroptosis remains to be investigated but is potentially another gasdermin.

<sup>b</sup>NLR4 activation by bacteria was observed to be accompanied by DNA fragmentation and laddering in wild-type cells (Miao et al., 2011). In contrast, (1) Pierini et al. (2012) and (2) Sagulenko et al. (2013) did not observe this phenomenon after stimulation of the AIM2 or NLRP3 inflammasome, respectively, in wild-type or ASC-deficient cells but instead only observed it in the absence caspase-1.

<sup>c</sup>Necroptosis occurs when caspase-8 is inhibited.

activated at the inflammasome, and in cells lacking caspase-1 protease activity, which suggests that this delayed, inflammasome-induced, LDH-releasing death in GSDMD-deficient cells is not driven by other potential substrates of caspase-1 (Figure 6B). In contrast, while the amount of IL-1 $\beta$  released from GSDMD-deficient cells eventually reached wild-type levels, cells lacking caspase-1 protease activity secreted less mature IL-1 $\beta$  even at late time points (Figures 6A and 6B), which is consistent with inefficient processing of IL-1 $\beta$  to the mature p17 form by caspase-8 (Maelfait et al., 2008) and the observation of additional IL-1 $\beta$  cleavage and degradation bands in cells lacking caspase-1 activity. Altogether, these results indicate that ineffective proteolytic processing of IL-1 $\beta$  accounts for reduced levels of mature IL-1 $\beta$  in the supernatant of cells lacking caspase-1 activ-

ity, while the alternative secretion mechanism engaged by the inflammasome in the absence of GSDMD cleavage by caspase-1 leads to the robust release of IL-1. The preservation of a certain degree of IL-1 processing and secretion in GSDMD-deficient cells would suggest that defects in caspase-1 activity should have a stronger effect than GSDMD deficiency *in vivo*. GSDMD-deficient mice displayed a less severe phenotype than did caspase-1 knockout mice during *F. novicida* infection (Figure 6C).

We next investigated the mechanism of inflammasome-induced lytic cell death that was observed in cells incapable of GSDMD-dependent pyroptosis (Table 1). Previous studies have shown that caspase-8 activation in caspase-1-deficient cells treated with inflammasome activators correlates with

### Figure 6. GSDMD-Dependent Pyroptosis Suppresses Caspase-8 Activation

(A) BMDCs of wild-type, *Gsdmd*<sup>−/−</sup>, *B6-Casp1*<sup>−/−</sup>, and *B6-Casp1*<sup>mt/mt</sup> mice were analyzed by immunoblot for caspase-8 processing, as well as maturation and secretion of IL-1 $\beta$  after inflammasome activation by nigericin or poly(dA:dT) for 3, 9, or 18 hr.

(B) Measurement of released IL-1 $\beta$  by ELISA and LDH by an enzymatic assay from samples in (A) (mean  $\pm$  SEM are shown).

(C) Following infection with *F. novicida* for 48 hr, bacterial loads in spleens (left) and livers (right) of wild-type, *Gsdmd*<sup>−/−</sup>, and *B6.129-Casp1* mice were determined by plating serial dilutions of organ homogenates on selective medium plates. The Mann-Whitney test was used for statistical analysis (\*p < 0.05, \*\*p < 0.01, \*\*\*p < 0.001, \*\*\*\*p < 0.0001). Spleen: *Gsdmd*<sup>−/−</sup> versus wild-type, p = 0.0017; *Gsdmd*<sup>−/−</sup> versus *B6.129-Casp1*<sup>−/−</sup>, p = 0.0014; wild-type versus *B6.129-Casp1*<sup>−/−</sup>, p < 0.0001; liver: *Gsdmd*<sup>−/−</sup> versus wild-type, p = 0.0004; *Gsdmd*<sup>−/−</sup> versus *B6.129-Casp1*<sup>−/−</sup>, p = 0.0189; wild-type versus *B6.129-Casp1*<sup>−/−</sup>, p < 0.0001; wild-type, *B6.129-Casp1*<sup>−/−</sup>, and *Gsdmd*<sup>−/−</sup>: n = 16.

(D) BMDCs from *B6.129-Casp1*<sup>mt/mt</sup> mice on chambered coverslips were stimulated with nigericin or 10  $\mu$ M raptinal and monitored for morphological changes over time by differential interference contrast (DIC) and fluorescence microscopy. Loss of membrane integrity was indicated by DRAQ7 (red) staining of DNA.

(E) BMDCs of wild-type, *B6.129-Casp1*<sup>−/−</sup>, and *Pycard*<sup>−/−</sup> mice were pretreated with the caspase inhibitors Z-VAD-fmk (20  $\mu$ M), IETD-fmk (30  $\mu$ M), or DEVD-fmk (30  $\mu$ M) and subsequently stimulated with nigericin. Lytic cell death was quantified by LDH release as measured by an enzymatic assay after 4, 8, 12, and 16 hr. In (A) and (B), data are representative of 2 independent experiments.

features of apoptosis such as activation of executioner caspases, nuclear condensation, DNA fragmentation, and phosphatidylserine exposure (Antonopoulos et al., 2015; Pierini et al., 2012; Puri et al., 2012; Sagulenko et al., 2013). Inflammasome activators triggered caspase-3 cleavage, PARP cleavage, and phosphatidylserine exposure in cells incapable of GSDMD-dependent pyroptosis (Figures 6A, S6B, and S6C; Table 1). As expected, inducers of apoptosis such as raptinal and doxorubicin triggered blebbing before loss of membrane integrity (Figures 6D and S6D). In contrast, cells incapable of GSDMD-dependent pyroptosis lost membrane integrity without prior blebbing upon treatment with inflammasome activators (Figure 6D). The loss of membrane integrity and the release of LDH by cells incapable of GSDMD-dependent pyroptosis indicate the existence of an alternative lytic cell death mechanism triggered by the inflammasome. The lack of blebbing suggests that this cell death pathway is not simply necrosis secondary to apoptosis, though the death modalities may employ the same upstream machinery. Several observations suggest that this lytic, inflammatory cell death pathway is not necroptosis: the robust activation of caspase-8 and caspase-3 (Figure 6A), the concomitant degradation of RIPK1 (Figure S5A), and the insensitivity to necrostatin-1 (Figure S6E). ASC deficiency markedly reduced lytic death at early and late phases, suggesting that the inflammasome platform is important not only for pyroptosis but also for this alternative lytic death pathway (Figures 6E and S6C). A bioluminescence assay revealed strong activation of caspases in cells lacking caspase-1 protease activity (Figure S6F). Furthermore, the pan-caspase inhibitor Z-VAD-fmk substantially (and to a lesser extent, the caspase-8 and caspase-3 inhibitors IETD-fmk and DEVD-fmk, respectively) reduced lytic death in cells lacking caspase-1 protease activity, suggesting that this form of cell death is driven by caspase activity (Figure 6E). The inability of these inhibitors to completely prevent lytic cell death is similar to the failure of peptide-based caspase-1 inhibitors to block GSDMD-dependent pyroptosis (Figure 3). Collectively, our data indicate that caspase-1 protease activity is required for pyroptosis and secretion of mature IL-1 at early time points after inflammasome activation. However, this study also demonstrates that in the absence of caspase-1 activity, the inflammasome activates caspase-8 and other caspases to trigger a GSDMD-independent secondary pyroptosis pathway as an alternative means to release mature IL-1.

## DISCUSSION

We have generated and analyzed mice expressing enzymatically inactive caspase-1<sup>C284A</sup>, which we have named *Casp1<sup>mit</sup>*. In contrast to the previous observation that biochemical inhibition of caspase-1 by peptide-based inhibitors selectively blocks IL-1 $\beta$  cleavage but does not prevent pyroptosis or IL-1 secretion (Broz et al., 2010; Cullen et al., 2015; Grob et al., 2012), genetic inactivation of caspase-1 protease activity prevented not only IL-1 $\beta$  cleavage but also canonical IL-1 secretion and pyroptosis at early time points after inflammasome activation. The inability of Ac-YVAD-cmk to block cleavage of the pyroptotic effector GSDMD explains this discrepancy. The inhibition of both arms of caspase-1 inflammatory activity—IL-1 secretion and pyroptosis—was recapitulated by VX-765, a second-generation pepti-

domimetic inhibitor of caspase-1. Peptide-based caspase inhibitors can block apoptosis and have therefore been key tools in apoptosis research. In contrast, our results speak to the limited utility of such inhibitors in studying pyroptosis, because residual caspase activity and gasdermin processing are sufficient for lytic cell death.

Additional facets of the interplay between caspase-1 and caspase-8 at the inflammasome were revealed by analysis of *Casp1<sup>mit</sup>* mice. Although caspase-1<sup>mit</sup> strongly accumulated at the inflammasome, inflammasomes containing caspase-1<sup>mit</sup> recruited and activated caspase-8 as effectively as naked, caspase-1-deficient inflammasomes. This suggests that caspase-1, which is recruited to ASC by a homotypic caspase recruitment domain (CARD) interaction, does not compete with caspase-8 for the same binding sites on ASC in native myeloid cell inflammasomes. Structural studies and inflammasome reconstitution experiments in HEK293T cells showed that caspase-8 is recruited via its tandem DED domains to the PYD domain of ASC (Fu et al., 2016; Pierini et al., 2012; Sagulenko et al., 2013; Vajjala et al., 2015). Mass spectrometry analysis of the inflammasome-enriched insoluble fraction demonstrated that ASC and caspase-1 were the most enriched proteins in this fraction. Detection of caspase-8 and other, less abundant components of the inflammasome will likely require improved enrichment methods.

Our data suggested that caspase-1 protease activity or its sequelae suppress caspase-8 activation at the inflammasome. Several substrates of caspase-1 have been identified (Agard et al., 2010; Denes et al., 2012), but deficiency of GSDMD alone allowed for simultaneous activation of caspase-8 and caspase-1 at the inflammasome. These findings imply that GSDMD-dependent pyroptosis, rather than caspase-1 activity per se, precludes inflammasome-induced activation of caspase-8. Further studies will be necessary to mechanistically explain how pyroptosis inhibits caspase-8 activation at the inflammasome. Our finding that inhibiting pyroptotic lysis does not restore caspase-8 activation in wild-type cells suggests an active signaling event might be involved.

In cells lacking caspase-1, activation of caspase-8 at the inflammasome has been implicated in the non-canonical maturation of IL-1 $\beta$  (Antonopoulos et al., 2015; Pierini et al., 2013). We observed the same phenomenon in cells specifically lacking caspase-1 protease activity. In line with previous *in vitro* cleavage assays (Maelfait et al., 2008), caspase-8-associated non-canonical processing of IL-1 $\beta$  in cells was less effective than caspase-1-mediated processing. In contrast to the rapid release of mature IL-1 $\beta$  from wild-type cells, IL-1 $\beta$  secretion from cells lacking caspase-1 protease activity was delayed. Despite this delay, GSDMD-deficient cells (in which caspase-1 is active) efficiently cleaved IL-1 $\beta$  and eventually released amounts of IL-1 $\beta$  equivalent to those released by wild-type cells. Thus, the non-canonical IL-1 release mechanism associated with caspase-8 activation and lytic cell death eventually compensated for the lack of rapid, caspase-1-driven, GSDMD-dependent release mechanisms. These findings also suggest that the ability of caspase-8 to contribute to IL-1-dependent inflammation may be limited by its inefficient cleavage of IL-1 $\beta$ . This is supported by our observation that intact caspase-1-mediated IL-1 $\beta$

processing in GSDMD-deficient mice correlates with enhanced protection of these mice relative to caspase-1-deficient mice during *Francisella* infection. Nonetheless, a role for caspase-8-driven non-canonical maturation and release of IL-1 in protection against infection is supported by previous *in vivo* studies showing that ASC-deficient mice (which lack both canonical and non-canonical IL-1 maturation and release pathways) are more susceptible to bacterial infection than caspase-1/11-deficient mice (Pierini et al., 2013). Collectively, these results suggest that alternative IL-1 maturation and release pathways contribute to immunity *in vivo*.

GSDMD-deficient cells are protected from caspase-11-driven cell death in response to intracellular LPS, even at late time points (Kayagaki et al., 2015; Shi et al., 2015). In contrast, we find that GSDMD-deficient cells treated with canonical activators that cause formation of an ASC-containing inflammasome are initially protected from cell death but lyse and release IL-1 after 8 hr. Though one possible explanation is that other caspase-1 cleavage targets mediate this alternative death pathway in GSDMD-deficient cells, our finding that delayed lytic death after inflammasome activation occurred with a similar strength and kinetics in GSDMD-deficient cells as in cells lacking caspase-1 protease activity demonstrates that caspase-1 protease activity is dispensable for this alternative lytic cell death modality. These results also raise the question of whether the formation of an ASC-containing inflammasome is a commitment to cell death. This issue may be worth considering in HIV infection, in which there is interest in using caspase-1 inhibitors to prevent pathogenic depletion of unproductively infected CD4<sup>+</sup> T cells (Doitsh et al., 2014). The inflammasome can serve as a platform for caspase-8 activation in CD4<sup>+</sup> T cells, so even effective caspase-1 inhibitors such as VX-765 may only delay HIV-induced death of these cells by diverting them to the slower alternative death pathway associated with caspase-8 activation (Martin et al., 2016). Therefore, in conditions such as HIV infection, cryopyrin-associated periodic syndromes, and sepsis, in which pyroptosis is implicated in pathogenic inflammation or cell depletion (Brydges et al., 2013; Kayagaki et al., 2011), it may be more effective to develop strategies to prevent formation of the inflammasome.

The inflammasome-induced delayed lytic cell death observed in cells incapable of GSDMD-dependent pyroptosis was driven by activation of caspase-8. Caspase-8 initiates the extrinsic apoptosis pathway by cleaving executioner caspases, which in turn degrade cellular proteins and kill the cell. Apoptosis is defined as an immunologically silent form of cell death; it preserves plasma membrane integrity and therefore does not release inflammatory cytokines or alarmins. Regulated necrosis pathways—including necroptosis, pyroptosis, and several other recently discovered cell death modalities—cause cell lysis but, in contrast to passive necrosis, are genetically controlled. Previous studies have classified inflammasome-induced cell death in caspase-1-deficient cells as apoptosis based on the observation of caspase-3 cleavage, phosphatidylserine exposure, nuclear condensation, and DNA degradation (Antonopoulos et al., 2015; Pierini et al., 2012; Puri et al., 2012; Sagulenko et al., 2013). Yet in contrast to apoptosis, inflammasome-induced cell death in cells lacking caspase-1 protease activity was lytic and released large amounts of IL-1. Its requirement for upstream

inflammasome components and its sensitivity to caspase inhibition demonstrate regulation. However, the lack of apoptotic blebbing before lysis suggests that this necrotic pathway was not simply secondary to apoptosis and therefore may represent a distinct form of regulated necrosis. On the basis of its specific features and its delay relative to canonical, caspase-1-dependent pyroptosis (Table 1), this lytic, inflammasome-dependent cell death might be considered a non-canonical or secondary form of pyroptosis. This adds another form of cell death to those already linked to caspase-8, raising the question how a molecule like caspase-8 has evolved such roles in diverse forms of cell death, including apoptosis, necroptosis, and secondary pyroptosis. This will be an intriguing topic for further study. The pore-forming gasdermin family member DFNA5 (Ding et al., 2016) was identified as a substrate of caspase-3 that executes secondary necrosis (Rogers et al., 2017) and lytic cell death in response to chemotherapeutics (Wang et al., 2017). DFNA5 is cleaved in parallel to other caspase substrates, so cell-type-specific differences in the balance of DNFA5 and executioners of apoptosis may govern the relative kinetics of classical apoptosis and regulated necrosis driven by apoptotic caspases. Cleavage of DFNA5 by caspase-3 may represent a mechanism by which caspase-8 activation at the inflammasome can cause secondary pyroptosis, but further research will be required to address this and other possible mechanisms.

## EXPERIMENTAL PROCEDURES

### Mice

*Nlrp3*<sup>-/-</sup>, B6.129-Casp1/11<sup>-/-</sup> (Kuida et al., 1995), B6.C-Tg(CMV-cre)<sup>1Cgn</sup>/J, *GSDMD*<sup>-/-</sup>, B6-Casp1<sup>mit/mit</sup>, B6.129-Casp1<sup>mit/mit</sup>, and B6-Casp1<sup>-/-</sup> mice were housed under SPF or SOPF conditions at the Zentrum für Präklinische Forschung (Munich, Germany), Charles River Laboratories (Italy), or the Biozentrum, University of Basel (Switzerland), in accordance with local and European guidelines, as well as Federation for Laboratory Animal Science Associations (FELASA) recommendations. *Casp1*<sup>mit</sup> mice were generated by conventional gene targeting in both C57BL/6 and 129 genetic backgrounds, and *Casp1*- and *GSDMD*-deficient mice were generated by CRISPR/Cas9 technology, as described in detail in the Supplemental Information.

### Reagents

All tissue culture reagents were from Invitrogen, unless indicated otherwise. Toll-like receptor (TLR) ligands were from InvivoGen. Raptinal was from AdipoGen Life Sciences. All other chemicals and reagents were from Sigma, unless indicated otherwise. Sources and identifiers of the antibodies used can be found in the Supplemental Information. *Salmonella enterica* subspecies I serovar Typhimurium X3625 (ΔaroA) (*Salmonella enterica* serovar Typhimurium) was a gift from Bärbel Stecher, Munich. Kits used for cloning were from Promega.

### Inflammasome Activation and Analysis

BMDCs were generated and stimulated as previously described (Groß et al., 2016; Schneider et al., 2013). Cells were primed with 50 ng/mL of ultrapure LPS for 3 hr, and inhibitors were added 30 min before stimulation with inflammasome activators at optimal concentrations, as outlined in the Supplemental Information. Stimulation with nigericin was performed with a final concentration of 5–10 μM and for a duration of 45–60 min. ELISA, immunoblot analysis, and other measurements were performed as described in detail in the Supplemental Information.

### Animal Infection

Infection of mice with wild-type *F. novicida* strain U112 was performed at the Biozentrum, University of Basel. All animal experiments were approved (license 2535-26742, Kantonales Veterinäramt Basel-Stadt) and were performed

according to local guidelines (Tierschutz-Verordnung, Basel-Stadt) and the Swiss animal protection law (Tierschutz-Gesetz). Bacteria were cultured overnight in brain heart infusion (BHI) medium (supplemented with 100 µg/mL ampicillin [AppliChem] and 0.2% L-cysteine). Bacteria were harvested by centrifugation and washed once with 1 × Dulbecco's Phosphate-Buffered Saline (DPBS). Mice were infected subcutaneously with  $5 \times 10^3$  CFU in 50 µL 1 × DPBS. Infected mice had access to food and water *ad libitum*. Mice were sacrificed 48 hr after infection, and spleen and liver were harvested. Colony-forming units (CFUs) were determined from spleen and liver homogenates plated in serial dilutions on Mueller-Hinton agar plates supplemented with 0.1% D-glucose (Millipore), 0.1% fetal calf serum (FCS) (BioConcept), 100 µg/mL ampicillin (AppliChem), and 0.1% L-cysteine. Statistical analysis was performed using GraphPad Prism 6.

### SUPPLEMENTAL INFORMATION

Supplemental Information includes Supplemental Experimental Procedures and six figures and can be found with this article online at <https://doi.org/10.1016/j.celrep.2017.12.018>.

### ACKNOWLEDGMENTS

The authors thank M. Yabal, P.J. Jost, and U. Maurer for helpful discussions and reagents; R. Megens and C. Weber, as well as J.-E. Heil and Y. Niyaz, for access to and support with using stimulated emission depletion (STED) and structured illumination microscopy (SIM) super-resolution microscopy equipment; and S. Weiß, V. Höfl, I. Spirer, N. Prayitno, and B. Lunk for technical assistance and mouse husbandry. This work was supported by a TUM Graduate School stipend (to K.S.S. and T.Č.); a postgraduate scholarship from the Natural Sciences and Engineering Research Council of Canada (to C.J.G.); the DFG (SFB 1054/B01 and RU 695/6-1 to J.R.); the Swiss National Science Foundation (PP00P3\_139120/1 to P.B.); the Bavarian Ministry of Sciences, Research and the Arts in the Framework of the Bavarian Molecular Biosystems Research Network (BioSysNet; to O. Groß); a European Research Council (ERC) Advanced Grant (322865 to J.R.); and an ERC Starting Grant (337689 to O. Groß).

### AUTHOR CONTRIBUTIONS

K.S.S., C.J.G., B.S.S., O. Gorka, J.S., and O. Groß designed and performed experiments and analyzed data. R.F.D., R.H., and E.M. performed and analyzed infection experiments. R.M. established and performed DIC and confocal and super-resolution fluorescence microscopy and analyzed the images. G.M. performed mass spectrometry analysis. R.N. performed blastocyst injection of *Casp1<sup>mt</sup>* embryonic stem cells and pro-nucleus injection of *Casp1*-targeting Cas9 gRNA. M.S.D. and T.Č. generated the *Gsdmd<sup>-/-</sup>* and *Casp1<sup>-/-</sup>* mice, respectively. P.B., J.R., and B.K. oversaw a portion of the work. K.S.S., R.M., and O. Groß prepared figures. C.J.G., K.S.S., and O. Groß wrote the paper, with input from all authors. O. Groß designed and oversaw the project.

### DECLARATION OF INTERESTS

B.K. is a founder and shareholder of OmicScouts, Freising, Germany.

Received: January 31, 2017

Revised: October 13, 2017

Accepted: December 4, 2017

Published: December 26, 2017

### REFERENCES

Agard, N.J., Maltby, D., and Wells, J.A. (2010). Inflammatory stimuli regulate caspase substrate profiles. *Mol. Cell. Proteomics* 9, 880–893.

Antonopoulos, C., El Sanadi, C., Kaiser, W.J., Mocarski, E.S., and Dubyak, G.R. (2013). Proapoptotic chemotherapeutic drugs induce noncanonical processing and release of IL-1β via caspase-8 in dendritic cells. *J. Immunol.* 191, 4789–4803.

Antonopoulos, C., Russo, H.M., El Sanadi, C., Martin, B.N., Li, X., Kaiser, W.J., Mocarski, E.S., and Dubyak, G.R. (2015). Caspase-8 as an effector and regulator of NLRP3 inflammasome signaling. *J. Biol. Chem.* 290, 20167–20184.

Brennan, M.A., and Cookson, B.T. (2000). *Salmonella* induces macrophage death by caspase-1-dependent necrosis. *Mol. Microbiol.* 38, 31–40.

Broz, P., and Dixit, V.M. (2016). Inflammasomes: mechanism of assembly, regulation and signalling. *Nat Rev Immunol.* 16, 407–420.

Broz, P., von Moltke, J., Jones, J.W., Vance, R.E., and Monack, D.M. (2010). Differential requirement for caspase-1 autoproteolysis in pathogen-induced cell death and cytokine processing. *Cell Host Microbe* 8, 471–483.

Brydges, S.D., Broderick, L., McGeough, M.D., Pena, C.A., Mueller, J.L., and Hoffman, H.M. (2013). Divergence of IL-1, IL-18, and cell death in NLRP3 inflammasomopathies. *J. Clin. Invest.* 123, 4695–4705.

Cullen, S.P., Kearney, C.J., Clancy, D.M., and Martin, S.J. (2015). Diverse activators of the NLRP3 inflammasome promote IL-1β secretion by triggering necrosis. *Cell Rep.* 11, 1535–1548.

Denes, A., Lopez-Castejon, G., and Brough, D. (2012). Caspase-1: is IL-1 just the tip of the ICEberg? *Cell Death Dis.* 3, e338.

Ding, J., Wang, K., Liu, W., She, Y., Sun, Q., Shi, J., Sun, H., Wang, D.-C., and Shao, F. (2016). Pore-forming activity and structural autoinhibition of the gasdermin family. *Nature* 535, 111–116.

Doitsh, G., Galloway, N.L.K., Geng, X., Yang, Z., Monroe, K.M., Zepeda, O., Hunt, P.W., Hatano, H., Sowinski, S., Muñoz-Arias, I., and Greene, W.C. (2014). Cell death by pyroptosis drives CD4 T-cell depletion in HIV-1 infection. *Nature* 505, 509–514.

Fernandes-Alnemri, T., Wu, J., Yu, J.-W., Datta, P., Miller, B., Jankowski, W., Rosenberg, S., Zhang, J., and Alnemri, E.S. (2007). The pyroptosome: a supramolecular assembly of ASC dimers mediating inflammatory cell death via caspase-1 activation. *Cell Death Differ.* 14, 1590–1604.

Fernandes-Alnemri, T., Yu, J.-W., Juliana, C., Solorzano, L., Kang, S., Wu, J., Datta, P., McCormick, M., Huang, L., McDermott, E., et al. (2010). The AIM2 inflammasome is critical for innate immunity to *Francisella tularensis*. *Nat. Immunol.* 11, 385–393.

Fu, T.-M., Li, Y., Lu, A., Li, Z., Vajjhala, P.R., Cruz, A.C., Srivastava, D.B., DiMaio, F., Penczek, P.A., Siegel, R.M., et al. (2016). Cryo-EM structure of caspase-8 tandem DED filament reveals assembly and regulation mechanisms of the death-inducing signaling complex. *Mol. Cell* 64, 236–250.

Galluzzi, L., López-Soto, A., Kumar, S., and Kroemer, G. (2016). Caspases connect cell-death signaling to organismal homeostasis. *Immunity* 44, 221–231.

Gewies, A., Gorka, O., Bergmann, H., Pechloff, K., Petermann, F., Jeltsch, K.M., Rudelius, M., Kriegsmann, M., Weichert, W., Horsch, M., et al. (2014). Uncoupling Malt1 threshold function from paracaspase activity results in destructive autoimmune inflammation. *Cell Rep.* 9, 1292–1305.

Groß, O., Yazdi, A.S., Thomas, C.J., Masin, M., Heinz, L.X., Guarda, G., Quadroni, M., Drexler, S.K., and Tschopp, J. (2012). Inflammasome activators induce interleukin-1α secretion via distinct pathways with differential requirement for the protease function of caspase-1. *Immunity* 36, 388–400.

Groß, C.J., Mishra, R., Schneider, K.S., Médard, G., Wettmarshausen, J., Dittlein, D.C., Shi, H., Gorka, O., Koenig, P.-A., Fromm, S., et al. (2016). K+ efflux-independent NLRP3 inflammasome activation by small molecules targeting mitochondria. *Immunity* 45, 761–773.

He, W.-T., Wan, H., Hu, L., Chen, P., Wang, X., Huang, Z., Yang, Z.-H., Zhong, C.-Q., and Han, J. (2015). Gasdermin D is an executor of pyroptosis and required for interleukin-1β secretion. *Cell Res.* 25, 1285–1298.

Kang, S., Fernandes-Alnemri, T., Rogers, C., Mayes, L., Wang, Y., Dillon, C., Roback, L., Kaiser, W., Oberst, A., Sagara, J., et al. (2015). Caspase-8 scaffolding function and MLKL regulate NLRP3 inflammasome activation downstream of TLR3. *Nat. Commun.* 6, 7515.

Kayagaki, N., Warming, S., Lamkanfi, M., Vande Walle, L., Louie, S., Dong, J., Newton, K., Qu, Y., Liu, J., Heldens, S., et al. (2011). Non-canonical inflammasome activation targets caspase-11. *Nature* 479, 117–121.

- Kayagaki, N., Stowe, I.B., Lee, B.L., O'Rourke, K., Anderson, K., Warming, S., Cuellar, T., Haley, B., Roose-Girma, M., Phung, Q.T., et al. (2015). Caspase-11 cleaves gasdermin D for non-canonical inflammasome signalling. *Nature* 526, 666–671.
- Kuida, K., Lippke, J.A., Ku, G., Harding, M.W., Livingston, D.J., Su, M.S., and Flavell, R.A. (1995). Altered cytokine export and apoptosis in mice deficient in interleukin-1 beta converting enzyme. *Science* 267, 2000–2003.
- Lemmers, B., Salmena, L., Bidère, N., Su, H., Matysiak-Zablocki, E., Murakami, K., Ohashi, P.S., Jurisicova, A., Lenardo, M., Hakem, R., and Hakem, A. (2007). Essential role for caspase-8 in Toll-like receptors and NFkappaB signaling. *J. Biol. Chem.* 282, 7416–7423.
- Liu, X., Zhang, Z., Ruan, J., Pan, Y., Magupalli, V.G., Wu, H., and Lieberman, J. (2016). Inflammasome-activated gasdermin D causes pyroptosis by forming membrane pores. *Nature* 535, 153–158.
- Luksch, H., Romanowski, M.J., Chara, O., Tüngler, V., Caffarena, E.R., Heymann, M.C., Lohse, P., Aksentijevich, I., Remmers, E.F., Flecks, S., et al. (2013). Naturally occurring genetic variants of human caspase-1 differ considerably in structure and the ability to activate interleukin-1 $\beta$ . *Hum. Mutat.* 34, 122–131.
- Maelfait, J., Vercammen, E., Janssens, S., Schotte, P., Haegman, M., Magez, S., and Beyaert, R. (2008). Stimulation of Toll-like receptor 3 and 4 induces interleukin-1 $\beta$  maturation by caspase-8. *J. Exp. Med.* 205, 1967–1973.
- Martin, B.N., Wang, C., Zhang, C.-J., Kang, Z., Gulen, M.F., Zepp, J.A., Zhao, J., Bian, G., Do, J.-S., Min, B., et al. (2016). T cell-intrinsic ASC critically promotes T<sub>H</sub>17-mediated experimental autoimmune encephalomyelitis. *Nat. Immunol.* 17, 583–592.
- Miao, E.A., Rajan, J.V., and Aderem, A. (2011). Caspase-1-induced pyroptotic cell death. *Immunol. Rev.* 243, 206–214.
- Philip, N.H., DeLaney, A., Peterson, L.W., Santos-Marrero, M., Grier, J.T., Sun, Y., Wynosky-Dolfi, M.A., Zwack, E.E., Hu, B., Olsen, T.M., et al. (2016). Activity of uncleaved caspase-8 controls anti-bacterial immune defense and TLR-induced cytokine production independent of cell death. *PLoS Pathog.* 12, e1005910–e1005930.
- Pierini, R., Juruj, C., Perret, M., Jones, C.L., Mangeot, P., Weiss, D.S., and Henry, T. (2012). AIM2/ASC triggers caspase-8-dependent apoptosis in *Francisella*-infected caspase-1-deficient macrophages. *Cell Death Differ.* 19, 1709–1721.
- Pierini, R., Perret, M., Djebali, S., Juruj, C., Michallet, M.-C., Förster, I., Marvel, J., Walzer, T., and Henry, T. (2013). ASC controls IFN- $\gamma$  levels in an IL-18-dependent manner in caspase-1-deficient mice infected with *Francisella novicida*. *J. Immunol.* 191, 3847–3857.
- Puri, A.W., Broz, P., Shen, A., Monack, D.M., and Bogoy, M. (2012). Caspase-1 activity is required to bypass macrophage apoptosis upon *Salmonella* infection. *Nat. Chem. Biol.* 8, 745–747.
- Rogers, C., Fernandes-Alnemri, T., Mayes, L., Alnemri, D., Cingolani, G., and Alnemri, E.S. (2017). Cleavage of DFNA5 by caspase-3 during apoptosis mediates progression to secondary necrotic/pyroptotic cell death. *Nat. Commun.* 8, 14128.
- Sagulenko, V., Thygesen, S.J., Sester, D.P., Idris, A., Cridland, J.A., Vajjhala, P.R., Roberts, T.L., Schroder, K., Vince, J.E., Hill, J.M., Silke, J., and Stacey, K.J. (2013). AIM2 and NLRP3 inflammasomes activate both apoptotic and pyroptotic death pathways via ASC. *Cell Death Differ.* 20, 1149–1160.
- Sborgi, L., Rühl, S., Mulvihill, E., Pipercevic, J., Heilig, R., Stahlberg, H., Farady, C.J., Müller, D.J., Broz, P., and Hiller, S. (2016). GSDMD membrane pore formation constitutes the mechanism of pyroptotic cell death. *EMBO J.* 35, 1766–1778.
- Schneider, K.S., Thomas, C.J., and Groß, O. (2013). Inflammasome activation and inhibition in primary murine bone marrow-derived cells, and assays for IL-1 $\alpha$ , IL-1 $\beta$ , and caspase-1. In *The Inflammasome. Methods in Molecular Biology*, C. De Nardo and E. Latz, eds. (Humana Press), pp. 117–135.
- Shi, J., Zhao, Y., Wang, K., Shi, X., Wang, Y., Huang, H., Zhuang, Y., Cai, T., Wang, F., and Shao, F. (2015). Cleavage of GSDMD by inflammatory caspases determines pyroptotic cell death. *Nature* 526, 660–665.
- Su, H., Bidère, N., Zheng, L., Cubre, A., Sakai, K., Dale, J., Salmena, L., Hakem, R., Straus, S., and Lenardo, M. (2005). Requirement for caspase-8 in NF-kappaB activation by antigen receptor. *Science* 307, 1465–1468.
- Thornberry, N.A., Bull, H.G., Calaycay, J.R., Chapman, K.T., Howard, A.D., Kostura, M.J., Miller, D.K., Molineaux, S.M., Weidner, J.R., Aunins, J., et al. (1992). A novel heterodimeric cysteine protease is required for interleukin-1 beta processing in monocytes. *Nature* 356, 768–774.
- Vajjhala, P.R., Lu, A., Brown, D.L., Pang, S.W., Sagulenko, V., Sester, D.P., Cridland, S.O., Hill, J.M., Schroder, K., Stow, J.L., et al. (2015). The inflammasome adaptor ASC induces procaspase-8 death effector domain filaments. *J. Biol. Chem.* 290, 29217–29230.
- Wang, Y., Gao, W., Shi, X., Ding, J., Liu, W., He, H., Wang, K., and Shao, F. (2017). Chemotherapy drugs induce pyroptosis through caspase-3 cleavage of a gasdermin. *Nature* 547, 99–103.
- Wannamaker, W., Davies, R., Namchuk, M., Pollard, J., Ford, P., Ku, G., Decker, C., Charifson, P., Weber, P., Germann, U.A., et al. (2007). (S)-1-((S)-2-([1-(4-amino-3-chloro-phenyl)-methanoyl]-amino)-3,3-dimethyl-butanoyl)-pyrrolidine-2-carboxylic acid ((2R,3S)-2-ethoxy-5-oxo-tetrahydro-furan-3-yl)-amide (VX-765), an orally available selective interleukin (IL)-converting enzyme/caspase-1 inhibitor, exhibits potent anti-inflammatory activities by inhibiting the release of IL-1 $\beta$  and IL-18. *J. Pharmacol. Exp. Ther.* 321, 509–516.

**Cell Reports, Volume 21**

**Supplemental Information**

**The Inflammasome Drives GSDMD-Independent  
Secondary Pyroptosis and IL-1 Release  
in the Absence of Caspase-1 Protease Activity**

**Katharina S. Schneider, Christina J. Groß, Roland F. Dreier, Benedikt S. Saller, Ritu Mishra, Oliver Gorka, Rosalie Heilig, Etienne Meunier, Mathias S. Dick, Tamara Ćiković, Jan Sodenkamp, Guillaume Médard, Ronald Naumann, Jürgen Ruland, Bernhard Kuster, Petr Broz, and Olaf Groß**

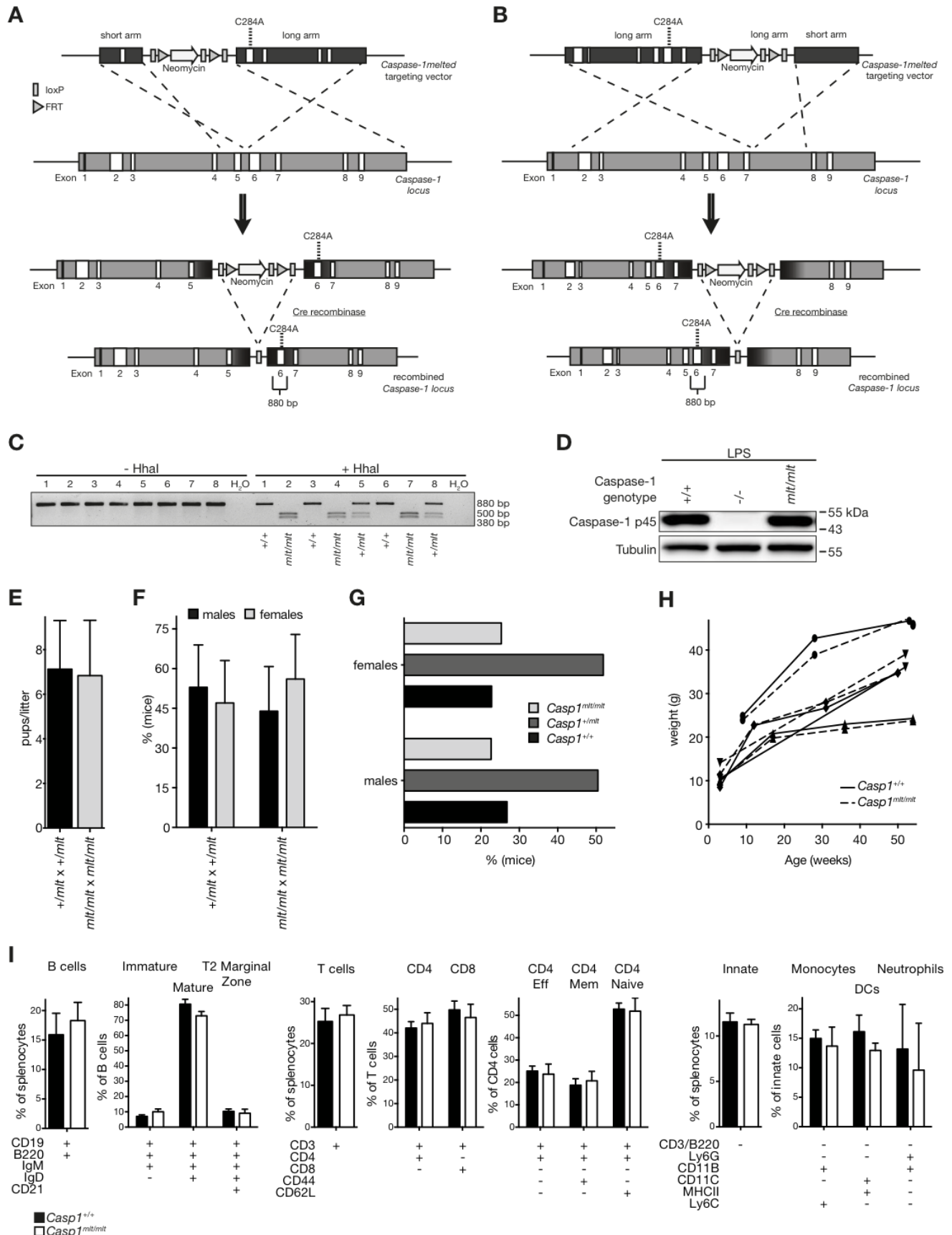


**Figure S1. Supplemental data corresponding to main Figure 1: Generation and characterization of *Casp1<sup>mit</sup>* mice**

(A, B) Schematics of the *Casp1<sup>mit</sup>* targeting strategies used in 129 (A) and C57BL/6 (B) stem cells. The region amplified by the genotyping PCR is indicated.

(C) Exemplary genotyping for the *Casp1<sup>mit</sup>* mutation by PCR. The restriction enzyme *HhaI* cuts the mutated site in the amplicon and results in two cleavage product bands in gel electrophoresis.

(D) Immunoblot analysis of caspase-1 protein expression in BMDCs from wild-type, B6.129-*Casp1<sup>-/-</sup>* and B6.129-*Casp1<sup>mit/mit</sup>* mice after LPS priming.

(E) Litter sizes of B6.129-*Casp1<sup>+/mit</sup>* x B6.129-*Casp1<sup>+/mit</sup>* breeding pairs were compared to B6.129-*Casp1<sup>mit/mit</sup>* x B6.129-*Casp1<sup>mit/mit</sup>*.

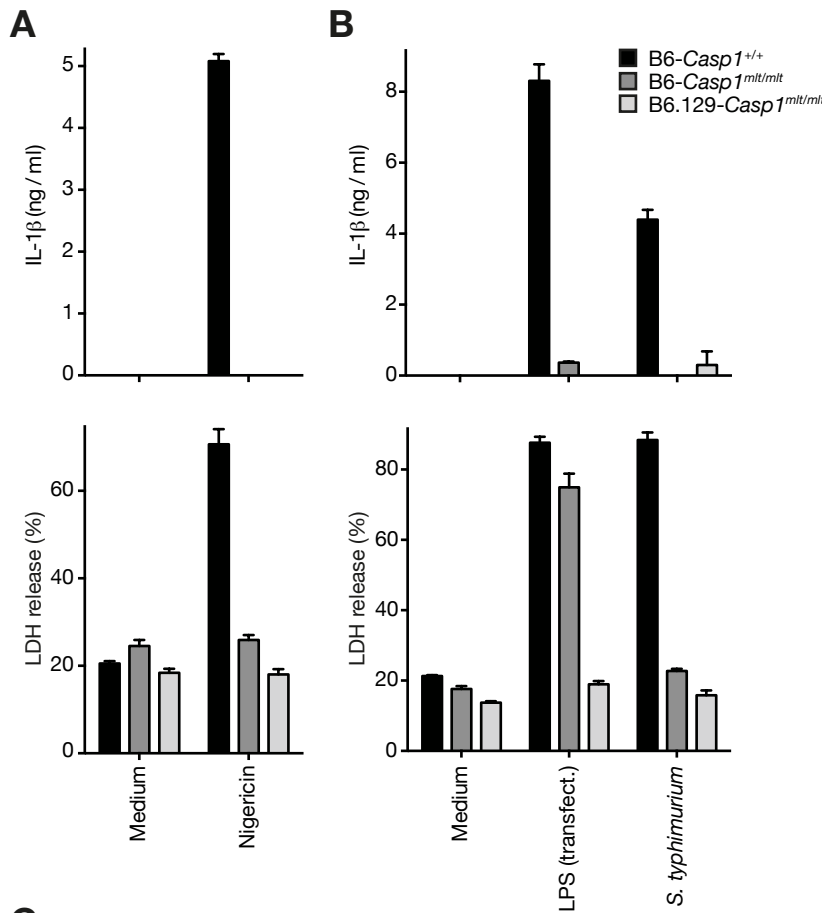
(F) Percentage of male and female pups born from heterozygous (B6.129-*Casp1<sup>+/mit</sup>* x B6.129-*Casp1<sup>+/mit</sup>*) or homozygous (B6.129-*Casp1<sup>mit/mit</sup>* x B6.129-*Casp1<sup>mit/mit</sup>*) *Casp1<sup>mit</sup>* breeding pairs.

(E and F) Heterozygous breeding pairs: n= 23, pups n= 183; homozygous breeding pairs: n= 8, pups n=69.

(G) Analysis of the distribution of *Casp1* genotypes in male and female pups born from heterozygous B6.129-*Casp1<sup>mit</sup>* breeding pairs (male pups n= 100; female pups n= 83).

(H) Weight development of four littermate pairs of one wild-type and one B6.129-*Casp1<sup>mit/mit</sup>* mouse each was monitored over  $\geq 50$  weeks.

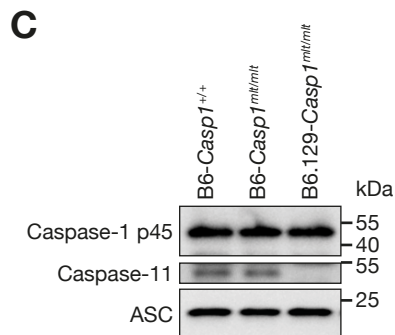
(I) Representative data from FACS analysis of various immune cell compartments from the spleens of wild-type and B6.129-*Casp1<sup>mit/mit</sup>* mice (n= 4 mice per group). Cells were phenotypically defined as indicated and are depicted as mean  $\pm$  s.d. of the indicated population.



**Figure S2. Supplemental data corresponding to main Figure 1: Non-canonical caspase-11 inflammasome activation in B6-Casp1<sup>mt</sup> cells**

(A, B) BMDCs derived from B6-Casp1<sup>+/+</sup>, B6-Casp1<sup>mt/mt</sup>, and B6.129-Casp1<sup>mt/mt</sup> mice were primed with 50 ng/ml LPS (A) or 1 μg/ml Pam3CSK4 (B) for 3h and subsequently stimulated with 5 μM nigericin for 45 min (A), transfected with 10 μg/ml LPS for 16h, or infected with *S. typhimurium* (MOI 20) for 2h (B). Secretion of IL-1β and release of LDH into the supernatant were measured by ELISA and with a colorimetric assay, respectively (mean ± s.e.m. are shown).

(C) BMDCs of the different genotypes as in A, B were analyzed by immunoblotting for the presence of caspase-1 and caspase-11.



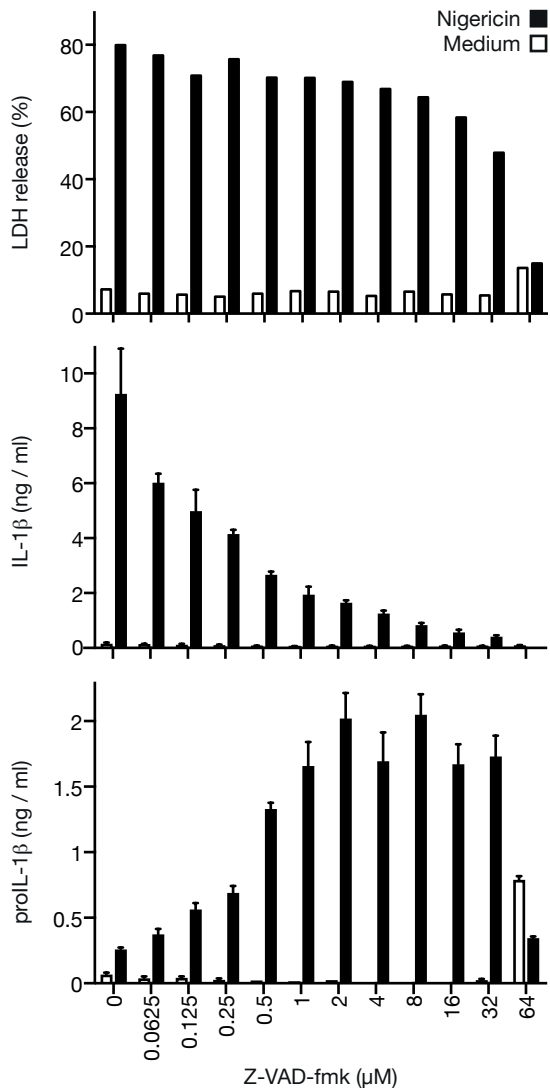


**Figure S3. Supplemental data corresponding to main Figure 3: Effect of Z-VAD-fmk on IL-1 $\beta$  secretion and cell viability**

Supernatants of wild-type BMDCs primed with 50 ng/ml LPS for 3h and stimulated with 5  $\mu$ M nigericin for 45 min were analyzed for secretion of proIL-1 $\beta$  and IL-1 $\beta$  by ELISA and release of LDH by an enzymatic assay in the presence of the indicated doses of the pan-caspase inhibitor Z-VAD-fmk (mean  $\pm$  s.e.m. are shown, data representative of two independent experiments).

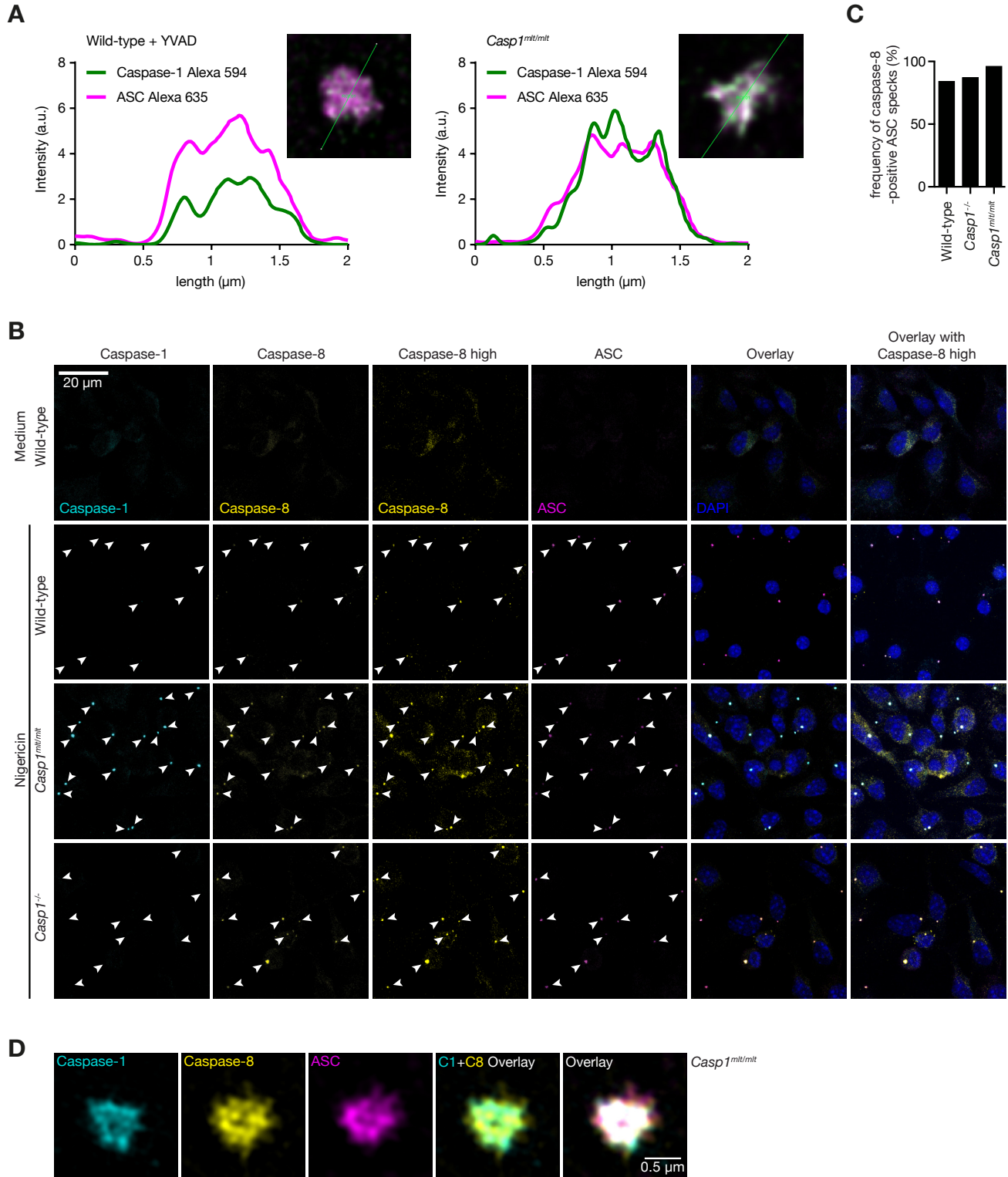


**Figure S4. Supplemental data corresponding to main Figure 4 and 5: Caspase-1<sup>mit</sup> and Caspase-8 accumulate at the inflammasome**

(A) Line intensity profiles of a region of interest of ASC specks from nigericin-stimulated wild-type + Ac-YVAD-cmk (left) or B6.129-Casp1<sup>mit/mit</sup> (right) BMDCs imaged by high resolution STED microscopy as in main Figure 4B. The graphs represent the intensities of caspase-1 (green) or ASC (magenta) at the line drawn in the speck.

(B) LPS-primed BMDCs from B6.129-Casp1<sup>mit/mit</sup> and -Casp1<sup>-/-</sup> mice on culture slides were stimulated with 10  $\mu$ M nigericin for 45 min or left unstimulated (medium) as in main Figure 5A. Cells were then fixed, immunofluorescence stained for caspase-1 (cyan), caspase-8 (yellow), and ASC (magenta), and confocal imaging was performed. DAPI (blue) localizes with the nuclei. Scale bar represents 20  $\mu$ m (data representative of >5 independent experiments). Caspase-8 images are depicted in two different signal intensities to allow evaluation of the frequency of caspase-8 recruitment to the ASC speck. ASC specks are indicated by arrows.

(C) Frequency of caspase-8 colocalization with ASC specks was determined in >100 specks from images obtained in four independent experiments.

(D) A slice through the middle of 3D projection of an ASC speck by SIM imaging depicting the arrangement of caspase-1 (cyan), caspase-8 (yellow) and ASC (magenta). LPS-primed BMDCs of B6.129-Casp1<sup>mit/mit</sup> mice on culture slides were stimulated with 10  $\mu$ M nigericin for 45 min, fixed, and immunofluorescence staining was performed. ASC speck was visualized at high resolution by 3D SIM imaging and z-sections were reconstructed as 3D projections.

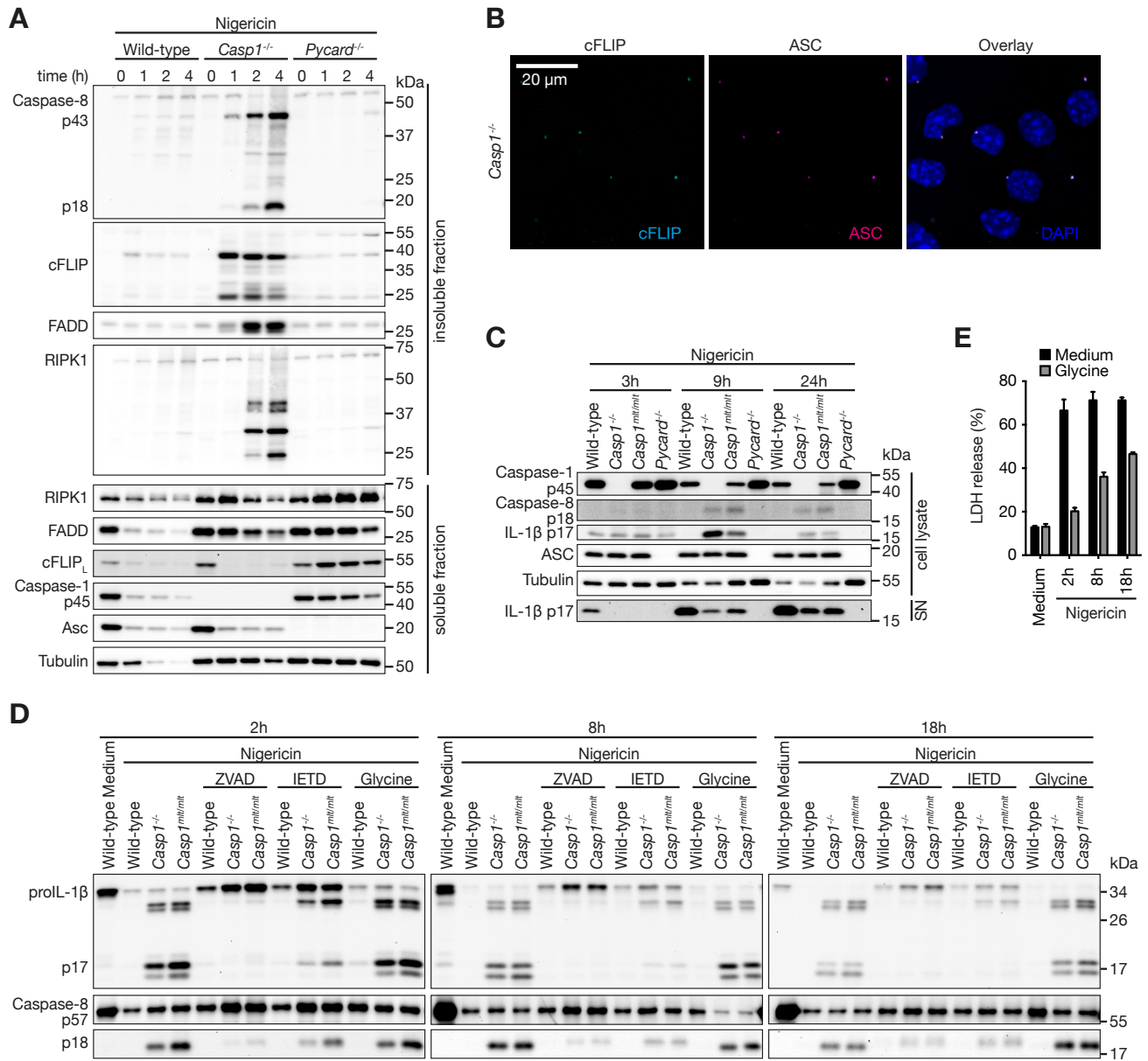


**Figure S5. Supplemental data corresponding to main Figure 5 and 6: Enhanced activation of caspase-8 in cells expressing caspase-1<sup>mit</sup>**

(A) BMDCs of wild-type, B6.129-Casp1<sup>-/-</sup>, and Pycard<sup>-/-</sup> mice were LPS-primed (50 ng/ml) for 3h and subsequently stimulated with 5 μM nigericin for up to 4h. NP-40-insoluble fractions of the cells were isolated by centrifugation and insoluble and soluble fractions analyzed by immunoblotting for presence and processing of caspase-8, cFLIP, FADD, RIPK1, caspase-1, and ASC.

(B) LPS-primed B6.129-Casp1<sup>-/-</sup> BMDCs on culture slides were stimulated with 10 μM nigericin for 45 min, fixed, and then immunofluorescence stained for cFLIP (cyan) and ASC (magenta), and confocal imaging was performed. DAPI (blue) localizes with the nuclei. Scale bar represents 20 μm.

(C) Immunoblot analysis of caspase-8, caspase-1, and IL-1 $\beta$  maturation and secretion up to 24h after inflammasome activation by 5  $\mu$ M nigericin in LPS-primed (50 ng/ml) BMDCs of inflammasome-competent vs. -incompetent mice as indicated (SN= supernatant; data representative of two independent experiments; B6-*Casp1<sup>mt/mt</sup>*).

(D) Immunoblot analysis of caspase-8 and pro-IL-1 $\beta$  maturation after inflammasome activation by 5  $\mu$ M nigericin in LPS-primed (50 ng/ml) B6-caspase-1 mutant BMDCs as indicated in the presence or absence of caspase inhibitors Z-VAD-fmk (20  $\mu$ M), IETD-fmk (20  $\mu$ M), or glycine (500  $\mu$ M; data representative of three independent experiments).

(E) LPS-primed wild-type BMDCs mice were pretreated with 500  $\mu$ M glycine and stimulated with nigericin (5  $\mu$ M) for 2, 8, and 18h. Release of LDH into the supernatant was assessed by an enzymatic assay.

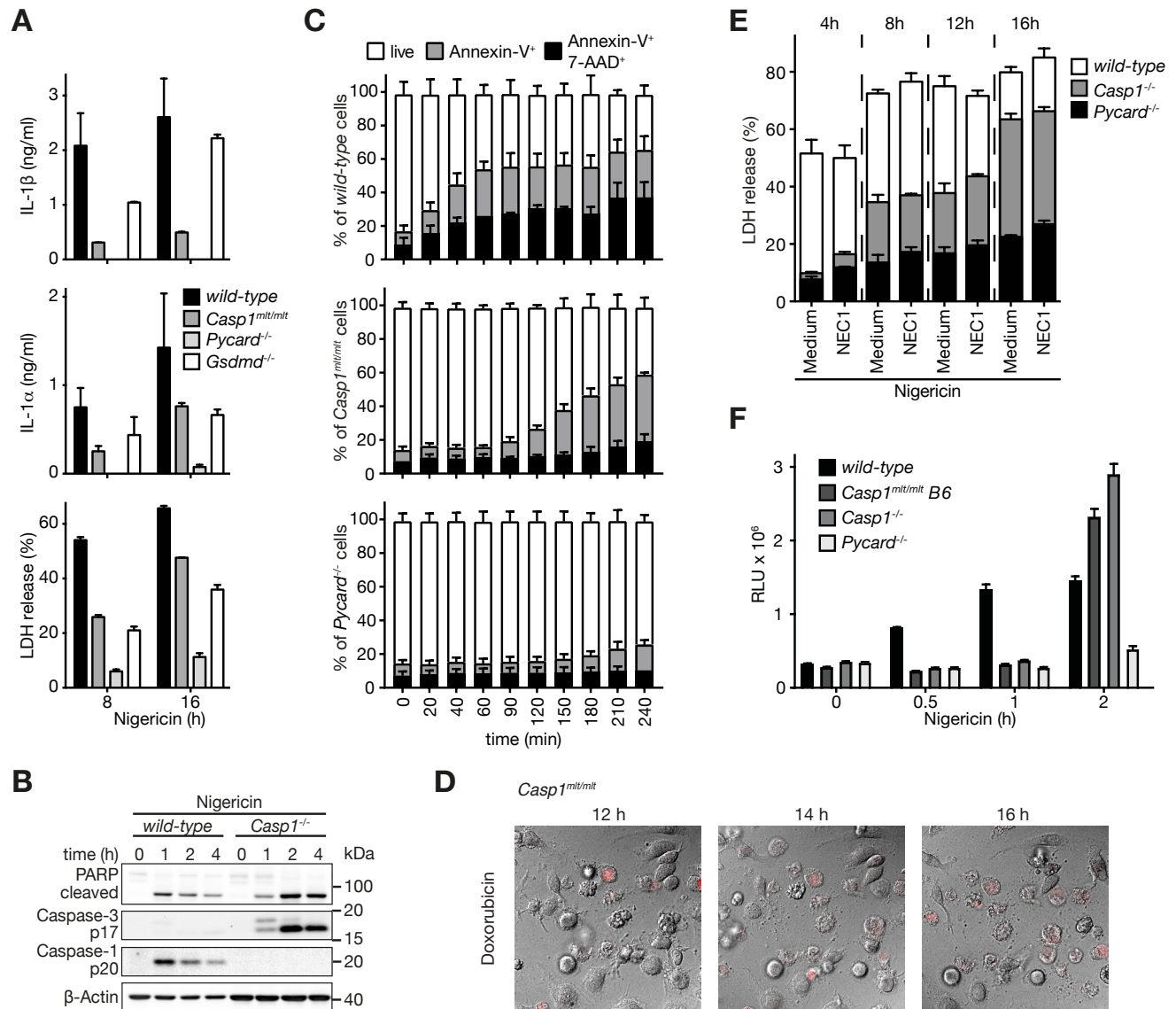


**Figure S6. Supplemental data corresponding to main Figure 6: GSDMD-dependent pyroptosis suppresses caspase-8 activation**

(A) BMDCs of wild-type, B6.129-*Casp1<sup>mlt/mlt</sup>*, *GSDMD<sup>-/-</sup>*, and *Pycard<sup>-/-</sup>* mice were LPS-primed and stimulated with nigericin (5  $\mu$ M) for 8 and 16h. Release of IL-1 $\beta$ , IL-1 $\alpha$ , and LDH into the supernatant were assessed by ELISA and an enzymatic assay, respectively.

(B) BMDCs from wild-type and B6.129-*Casp1<sup>-/-</sup>* mice were LPS-primed (50 ng/ml) for 3h and subsequently stimulated with 5  $\mu$ M nigericin for up to 4h and analyzed by immunoblotting for presence of the processed form of PARP, caspase-3, and caspase-1.

(C) Viability of LPS-primed BMDCs of wild-type, B6-*Casp1<sup>mlt/mlt</sup>*, and *Pycard<sup>-/-</sup>* mice stimulated with nigericin (5  $\mu$ M) for the indicated time-points. Cells were harvested simultaneously and stained for Annexin-V and 7-AAD before analysis by flow cytometry. The bar graphs show the stacked percentages of live (Annexin-V<sup>neg</sup> 7-AAD<sup>neg</sup>), Annexin-V<sup>+</sup>, and Annexin-V<sup>+</sup> 7-AAD<sup>+</sup> cells for the given genotypes (mean  $\pm$  s.d. of three independent experiments).

(D) LPS-primed BMDCs from B6.129-*Casp1<sup>mtl/mtl</sup>* mice on glass chambered coverslips as in Figure 6D were stimulated with doxorubicin and monitored for morphological changes for up to 16h by DIC and fluorescence microscopy. DRAQ7 (red) stains DNA upon loss of membrane integrity.

(E) Lytic cell death over time as indicated was compared by means of LDH release from BMDCs of wild-type, B6.129-*Casp1<sup>-/-</sup>*, and *Pycard<sup>-/-</sup>* mice, which were LPS-primed and nigericin-stimulated in the presence or absence of the necroptosis inhibitor Nec-1.

(F) LPS-primed BMDCs of the indicated genotypes were activated with nigericin (5  $\mu$ M); cleavage of a synthetic caspase-1 substrate was assessed by luminescent emission 0, 0.5, 1, and 2h after stimulation.

## SUPPLEMENTAL EXPERIMENTAL PROCEDURES

### Generation of *Casp1<sup>mt</sup>* mice

A fragment of the murine *Casp1* gene was amplified by PCR from BAC clone RP23-424D5 (Source Bioscience) originating from a C57BL/6 mouse and used as a short arm (SA) for homologous recombination. The GCATGCCGT to GCAGCGCGT mutation at codon 284 was introduced into the long arm (LA) cloned from the same BAC template. Both fragments were cloned into the targeting vector pSPUC-DTA (Gewies et al., 2014). Sequence integrity was controlled by sequencing at GATC Biotech AG, Germany. *NotI*-linearized targeting vector was electroporated into R1/E (129S1/X1) or C57BL/6N embryonic stem cells. G418-resistant embryonic stem cells were screened by PCR combined with *HhaI* digest and Southern blot analysis. Clones that showed correct genomic integration of the targeting vector and presence of the *Casp1<sup>mt</sup>* mutation were injected into C57BL/6 blastocysts, which yielded chimeric males that displayed germline transmission of the *Casp1<sup>mt</sup>* allele. The floxed neomycin resistance cassette between exons 5 and 6 was removed by breeding to DEL-Cre mice (B6.C-Tg(CMV-cre)<sup>1Cgn</sup>/J), and the resulting mice were backcrossed 8 generations to the C57BL/6 background. Routine genotyping was performed by *HhaI* digest of PCR products amplified with the following primers: 5'- CCAAGGGAATTATTGCTGTCTTG-3' and 5'- GTGATATTCTGTGGTGACTAACCGA-3'.

### Generation of *Casp1<sup>-/-</sup>* in C57BL6 mice

Guide RNAs targeting exon 5 of the mouse *Casp1* gene were designed as described (Kayagaki et al., 2015) using the CRISPR Design website at <http://crispr.mit.edu> and ordered from Sigma Aldrich in RNA format using the gRNA sequence (including PAM) with the inverse sequence GAGGGCAAGACGTGTACGAGTGG (target ID: MM0000278298). Pronucleus injection of the gRNAs and Cas9 protein was done as described before (Hermann et al., 2014). The founders were screened by amplifying the region of interest by PCR with high-fidelity Phusion DNA Polymerase (ThermoFisher Scientific) and subsequent sequencing of the PCR product (GATC Biotech AG) using primers *Casp1\_E5 <sup>fwd</sup>*: TAGGAATTCGATGCTGAGAGCCTACCAGG and *Casp1\_E5 <sup>rev</sup>*: TCAGAATTCACCAGTACAGAACTAGCAAGGC, containing *EcoRI* restriction sites (underlined). Results were analyzed using CLC Main Workbench. Mice showing a heterogeneous DNA sequence in the region of interest were chosen for further analysis. To that end, the PCR product was cloned into the pCR2.1-TOPO TA vector (Thermo Fisher Scientific) and transformed into DH5 $\alpha$  *E. coli* (NEB). DNA was isolated from seven different clones, sequenced, and analyzed for mutations causing a premature stop codon. The founder chosen for further breeding showed a TT insertion on one allele, leading to a translation stop in exon 5 of the *Casp1* gene. In addition, this mutation introduced a *BsrGI* restriction site (T  $\nabla$  GTACA). For genotyping the offspring, this restriction enzyme (NEB) was used on PCR products generated with the above-mentioned primers.

### Generation of *Gsdmd<sup>-/-</sup>* mice

Guide RNAs targeting exon 2 of the mouse *Gsdmd* gene were designed as described (Kayagaki et al., 2015) using gRNA sequence (including PAM) GGAGAAGGGAAAATTTCTGG. Injection of the gRNAs and Cas9 protein into C57BL/6 embryos was done as described before (Hermann et al., 2014). Biopsies for genotyping were taken at an age of 10-12 days. DNA extraction was performed using the KAPA HotStart Mouse Genotyping Kit according to the manufacturer's protocol. Genotyping PCR was done using Q5 Polymerase (NEB) using primers Oligo.507 (GSDMD\_ex2\_fw2; ggtgtgagccaccgtctat) and Oligo.508 (GSDMD\_ex\_rv2; ctgtggagggactccattgt), which were designed using Primer3 v.0.4.0 (<http://bioinfo.ut.ee/primer3-0.4.0/primer3/>), resulting in a fragment of 768 bp. The PCR product was sequenced using Oligo.507. This led to a 2 bp deletion in exon 2 of *Gsdmd* resulting in a premature stop codon.

### BMDC preparation and stimulation

Bone marrow-derived dendritic cells (BMDCs) were prepared from the tibiae and femora of 6-30 weeks old mice as previously reported (Groß et al., 2016; Schneider et al., 2013). Cells were grown in a humidified incubator at 37°C / 5% CO<sub>2</sub> in the presence of recombinant murine GM-CSF (20 ng/ml, Immunotools). After 6-9 days of differentiation, cells were harvested using 5 mM EDTA in 1x HBSS buffer and plated in 96-well plates at a density of 0.12-0.2 x 10<sup>6</sup> cells per well in medium containing growth factor.

For stimulation of TLRs, cells were treated for 6h with the following concentrations of agonists: 20 ng/ml LPS, 10  $\mu$ g/ml CpG DNA, 1  $\mu$ g/ml R848, 0.1  $\mu$ g/ml Pam<sub>3</sub>CSK<sub>4</sub>, 0.1 mg/ml Zymosan, 0.1 mg/ml Curdlan

(Wako). For inflammasome activation, cells were primed with 50 ng/ml *E.coli* K12 ultra-pure LPS for 3 hours and subsequently stimulated with inflammasome activators for 0.5-24h. Typical concentrations and incubation times if not indicated otherwise were as follows: 5  $\mu$ M nigericin (10  $\mu$ M for microscopy) for 45-60 min, 1  $\mu$ g/ml poly(dA:dT) for 3h (transfected with Lipofectamine 2000), 70  $\mu$ M Imiquimod for 2-3h, and MOI 20 *S. typhimurium* for 1-2h. For stimulation using bacteria, sterile LB-medium without antibiotics was inoculated with *Salmonella enterica* subspecies I serovar Typhimurium X3625 ( $\Delta$ aroA) (*S. typhimurium*) from a glycerol stock. After 12h at 37°C and 250 rpm, bacteria were subcultured in LB-medium diluted 1:20, 1:40, and 1:80 for another 3h at the same conditions. Samples with exponential growth rates (leading to Nlrp4-dependent, caspase-11 / Nlrp3-independent inflammasome activation, as previously described (Broz *et al.*, 2012)) were selected by measuring OD<sub>600</sub> using a BioPhotometer plus. Bacterial numbers were estimated by assuming OD<sub>600</sub> = 0.1 = 1  $\times$  10<sup>8</sup> colony-forming-units (cfu) per ml.

The caspase inhibitors Ac-YVAD-cmk (Enzo), Z-VAD-fmk (Enzo), Z-IETD-fmk (BioTechne), and VX-765 (a gift from Boehringer Ingelheim) were added to the cells at a concentration of 0.03-100  $\mu$ M as indicated after 2.5h of priming and 30 min prior to inflammasome activation. All inflammasome activators were carefully titrated and used at the lowest dose and the shortest time required to cause significant IL-1 secretion. All stimulations were performed in triplicates.

### Analysis of BMDC stimulations

Cytokines were quantified from cell-free supernatants by ELISA for murine IL-1 $\alpha$ , IL-1 $\beta$ , pro-IL-1 $\beta$  and TNF according to manufacturer's instructions (eBioscience). The IL-1 $\beta$  ELISA used is selective for the mature form of mouse IL-1 $\beta$ , while the pro-IL-1 $\beta$  ELISA only detects the pro-form since one of the antibodies is directed against the pro-domain (Dick *et al.*, 2016; Groß *et al.*, 2012; Schneider *et al.*, 2013). Cells were stimulated and measured in triplicates and values are shown as mean  $\pm$  s.e.m. (technical triplicates). For immunoblot analysis, triplicates of cell-free supernatants were pooled and combined with 3x SDS- and DTT-containing sample buffer (Schneider *et al.*, 2013). Cell lysates were prepared by washing cells with PBS and lysing them in the well in 1x sample buffer and pooling the triplicates. Supernatants and lysates were subjected to SDS-PAGE and transferred to nitrocellulose using standard techniques (Schneider *et al.*, 2013). To analyze inflammasome formation, the insoluble fraction of NP-40-lysed cells was subjected to immunoblot analysis, as previously described (Fernandes-Alnemri *et al.*, 2007). For immunoblotting of GSDMD, cytoplasmic fractions were prepared from BMDCs. 2  $\times$  10<sup>6</sup> cells were lysed in 100  $\mu$ l NP-40-containing lysis buffer and lysates were depleted of membranes by centrifugation to obtain cytoplasmic fractions.

Primary antibodies were as follows: goat anti-mouse IL-1 $\beta$  (AF-401, R&D Systems), mouse anti-mouse caspase-1 p20 (Casper-1, AdipoGen Life Sciences), mouse anti-mouse caspase-1 (Casper-2, AdipoGen Life Sciences), rabbit anti-ASC (AL177, AdipoGen Life Sciences), rat anti-mouse caspase-8 (1G12, Enzo), rabbit anti-mouse caspase-3 (#9661 and #9662, Cell Signaling), rabbit anti-GSDMD (G7422, Sigma), mouse anti- $\alpha$ -tubulin (B512, Sigma), rabbit anti-Vimentin (D21H3, Cell Signaling).

Cell death was determined by measuring LDH using the Promega CytoTox 96 Non-Radioactive Cytotoxicity kit according to the protocol. Medium served as blank value and was subtracted from the sample values. Results were plotted as percentage of 100 % dead cells lysed by repeated freeze-thaw cycles.

Caspase activity was analyzed by using the Promega CaspaseGlo® 1 Inflammasome assay according to the manufacturer's specifications. Cells were plated in white-walled 96-well plates and stimulated with nigericin for the indicated times. Medium without cells served as blank value and was subtracted from sample values. Luminescence was measured using a Mithras multimode microplate reader (Berthold).

For viability time course experiments, BMDCs were plated in 96 well cell culture plates (1 $\times$ 10<sup>5</sup> cells/well), cultured overnight at 37°C, primed with 50 ng/ml LPS for at least 3h and stimulated with nigericin (5  $\mu$ M) for various time-points up to 240 min. Cells were simultaneously harvested from plates by washing with 1x DPBS with 5 mM EDTA and stained with Annexin-V Pacific Blue 7-AAD Apoptosis Detection Kit (Biolegend). Samples were measured on a FACS Canto II (BD) and analyzed using FlowJo (FlowJo, LLC).

For membrane integrity experiments, BMDCs were seeded at 3 $\times$ 10<sup>5</sup> cells/well in 8-well chambered coverslips (Ibidi), cultured overnight at 37°C, and primed with 50 ng/ml LPS for at least 3h. Nigericin (5  $\mu$ M), raptinal (10  $\mu$ M), or doxorubicin (10  $\mu$ M) were prepared in FCS supplemented phenol-red free FluoroBrite DMEM medium containing DRAQ7 (3  $\mu$ M). Following stimulation, cellular morphology (by DIC) and membrane integrity (by fluorescence imaging) were continuously observed for a time course of up to 16h by confocal microscopy on a Leica TCS SP8 confocal LSM equipped with a 63 $\times$  oil objective (NA 1.4, Leica Microsystems). The staining of the DNA by DRAQ7 indicated plasma membrane leakage.

## Immunophenotyping

Four 8 weeks-old *Casp1*<sup>+/+</sup> and B6.129-*Casp1*<sup>mit/mit</sup> mice each were sacrificed and spleens and cervical, axillary, and inguinal lymph nodes were harvested. Mice and organs were weighed, organs meshed, and red blood cell lysis was performed using G-DEX™ II RBC Lysis Buffer. Cells were counted using a hemocytometer and  $1.5 \times 10^6$  cells per organ were antibody-stained on a 96-V-bottom plate. First, cells were resuspended in live/dead stain eFluor 506 (1:1000 in 1x DPBS) and incubated for 10 min at 4°C in the dark. After that cells were washed and incubated in antibody mixtures for 30 min at 4°C in the dark. Cells were washed two times before immediate acquisition. All antibodies were diluted 1:400 in 1x DPBS + 2 % FCS except for anti-CD16/CD32, which was used at 1:200. Samples were analyzed by a FACS Canto II (BD Biosciences), data acquired by the DIVA software (BD Biosciences), and evaluated using FlowJo software (FlowJo, LLC). Compensation was performed using cells labeled with the corresponding antibodies for all conjugates according to the manufacturer's protocol. All antibodies were from eBioscience [eB] and Biolegend [BL]. Antibodies used were as follows: rat anti-mouse CD11c APC-conjugated (N418) [eB], rat anti-mouse CD16/CD23 (clone 93) [eB], rat anti-mouse CD19 eFluor 450-conjugated (1D3) [eB], rat anti-mouse CD21 FITC-conjugated (4E3) [eB], rat anti-mouse CD4 eFluor 450-conjugated (RM4-5) [eB], rat anti-mouse CD8 APC-conjugated (53-6.7) [eB], rat anti-mouse IgD APC-conjugated (11-26c) [eB], rat anti-mouse IgM PE-Cy5-conjugated (II/41) [eB], rat anti-mouse Ly6C PerCP-Cy5.5-conjugated (HK1.4) [BL], rat anti-mouse Ly6G PE-conjugated (1A8) [BL], rat anti-mouse CD11b PE-Cy7-conjugated (M1/70) [BL], rat anti-mouse CD11c APC-conjugated (N418) [BL], rat anti-mouse CD62L PerCP-Cy5.5-conjugated (MEL-14) [eB], rat anti-mouse CD44 APC-Cy7-conjugated (IM7) [eB], rat anti-mouse CD3 FITC-conjugated (17A2) [eB], rat anti-mouse B220 FITC-conjugated (RA3-6B2) [eB], rat anti-mouse B220 APC-Cy7-conjugated (RA3-6B2) [eB], rat anti-mouse I-A/I-E APC-Cy7-conjugated (M5/114.15.2) [BL].

## Immunofluorescence Imaging

For confocal immunofluorescence imaging of the ASC inflammasome, murine BMDCs were seeded at  $2 \times 10^5$  cells/well in 12-well culture slides (Ibidi). Cells were primed with 50 ng/ml of LPS for 2h and then stimulated with nigericin (10  $\mu$ M for 45 min) or left unstimulated. After treatment, the cells were washed with 1x DPBS, fixed in 4% paraformaldehyde for 10 min, and extracted in 1x DPBS with 0.1% (v/v) Triton-X100 for 5 min. Non-specific interactions were minimized by blocking with buffer containing 5% FCS and 0.1% Triton X-100 in 1x DPBS. Cells were stained overnight at 4°C with mouse anti-mouse caspase-1 (p10) (Casper-2, AdipoGen Life Sciences), rabbit anti-ASC antibody (AL177, AdipoGen Life Sciences), and (where mentioned) rat anti-mouse caspase 8 (1G12, Enzo) or rat anti-FLIP (Dave-2, Adipogen Life Sciences) diluted in blocking buffer. The anti-mouse Alexa Fluor 488 and anti-rabbit Alexa Fluor 555 were applied as secondary antibodies for double labelling while anti-mouse Alexa Fluor 488, anti-rat Alexa Fluor 555, and anti-rabbit Alexa Fluor 647 were used for triple staining at ambient temperature. All secondary antibodies were from Thermo Fisher Scientific. The slides were mounted in Prolong Diamond containing DAPI (Thermo Fisher Scientific). Confocal microscopy of immunostained cells was performed on a Leica TCS SP8 confocal LSM equipped with a 63x oil objective (NA 1.4) oil objective (Leica Microsystems) keeping the laser settings for imaging constant between samples for comparison. The images were acquired as z-stacks and compiled as maximum projection in 2D for display using the LAS X software package (Leica, Germany).

For improved optical resolution ( $\approx$  100 nm), the double labelled samples were also observed with an ELYRA PS.1 (Carl Zeiss Microimaging) microscope for structured illumination microscopy (SIM). Caspase-1 (p10) was labelled with anti-mouse Alexa Fluor 488 and ASC with anti-rat Alexa Fluor 555. Thin z-sections of ASC specks were collected in five rotations for each channel. Images were reconstructed using ZEN software (Carl Zeiss MicroImaging).

For higher optical resolution (<100 nm), stimulated emission depletion (STED) imaging was performed to better visualize the arrangement of caspase-1 and ASC in the ASC speck. Murine BMDCs were treated, fixed, extracted, blocked, and stained with primary antibodies towards caspase-1 (p10) and ASC as detailed above. The anti-mouse Alexa Fluor 594 and anti-rabbit Alexa Fluor 635 were applied as secondary antibodies (1:100 dilution) and 3D STED imaging was performed using a Leica SP8 STED 3X (Leica, Germany) equipped with a 100x oil objective (NA 1.4). A tunable white light laser source was used to optimally excite the applied fluorophores while depletion was performed at 775 nm for both Alexa Fluor 594 and Alexa Fluor 633. Images were collected in a sequential scanning mode using hybrid diode detectors to maximize signal collection while reducing background noise and the cross-talk between the channels. Image reconstructions were performed using the LAS X software package (Leica, Germany) and deconvolution was applied with the Huygens

Professional software package (Scientific Volume, the Netherlands). Line intensity profiles were also generated in LAS X software by drawing a line passing across the ASC speck.

### Mass Spectrometry Analysis

BMDCs from B6.129-*Casp1<sup>mit/mit</sup>*, -*Casp1<sup>-/-</sup>* and *Nlrp3<sup>-/-</sup>* mice were plated at  $1.5 \times 10^7$  cells per 100 mm plate and primed with 20 ng/ml LPS for 3h. Afterwards, four plates per genotype were treated with 5  $\mu$ M nigericin for 40 min and one plate each was left untreated. Replicates were kept individually at all times. Cell lysates, soluble and insoluble fractions of NP-40-lysed cells were prepared in SDS- and DTT-containing sample buffer as described above and subjected to SDS-PAGE. Proteins in the gel were visualized by Coomassie staining according to standard procedures and the protein amount per sample was estimated from comparison to a BSA-standard loaded onto the same gel. An equivalent of 8  $\mu$ g protein were subjected to alkylation with 55 mM chloroacetamide for 30 minutes and immediately afterwards, SDS-PAGE was performed. NuPAGE 4-20% Bis-Tris gels and NuPAGE MES SDS Running Buffer (both from Invitrogen) were used and electrophoresis was stopped as soon as the samples had entered the separating gel. Coomassie staining was done and the gel stored in 1 % acetic acid at 4°C until mass spectrometry analysis.

LC-MS/MS measurements were performed on an Eksigent nanoLC-Ultra 1D+ system (Eksigent, Dublin, CA) coupled to an Orbitrap Velos mass spectrometer (Thermo Fisher Scientific, Bremen, Germany). The dried samples were reconstituted in 20  $\mu$ L 0.1% FA, one half was loaded onto a trap column (100  $\mu$ m x 2 cm, packed in-house with 5  $\mu$ m C18 resin, Reprosil-PUR AQ material, Dr. Maisch) and washed using 0.1% FA for 10 min at a flow rate of 5  $\mu$ L/min. Accordingly, peptides were transferred to an analytical column (75  $\mu$ m x 40 cm, packed in-house with 3  $\mu$ m C18 resin, Reprosil-Gold C18 material, Dr. Maisch). During separation using a 225 min gradient from 4% to 32% solvent B (0.1% FA, 5% DMSO in 100% ACN) in solvent A (0.1% FA, 5% DMSO in HPLC-grade water) (Hahne *et al.*, 2013) at 300 nl/min flow rate, samples were directly injected into the Velos via ESI in positive ionization mode. The Velos was operated in DDA mode, automatically switching between MS1 and MS2 spectra both acquired in the Orbitrap mass analyzer. Full scan MS1 spectra (m/z 360 to 1300) were generated at a resolution of 30 000 using an automatic gain control (AGC) target value of 1e6 charges with a maximum injection time of 200 ms. Internal calibration was performed using a dimethyl sulfoxide cluster (m/z 401.922720). The top 10 peptide precursor peaks (isolation window 2 Th) were fragmented via HCD in the collision cell (normalized collision energy of 30%) using an AGC target value of 3e4 with a maximum injection time of 200 ms. Fragment ions (fixed first mass of 100 m/z) were recorded at a resolution of 7500 and dynamic exclusion was set to 20 s. Data analysis was performed using MaxQuant (version 1.5.1.0) (Cox and Mann, 2008) with the integrated search engine Andromeda (Cox *et al.*, 2011). For peptide and protein identification, raw files were searched against the UniProt mouse (010090) reference database (version 06/06/2014) annotated with Pfam. Carbamidomethylated cysteine was selected as fixed modification and oxidation of methionine as well as N-terminal protein acetylation as variable modification. Trypsin/P was selected as the proteolytic enzyme, with up to two missed cleavage sites allowed. Precursor tolerance was set to 6 ppm, and fragment ion tolerance, to 20 ppm. Peptide identifications required a minimal length of seven amino acids, and all data sets were adjusted to 1% PSM and 1% protein FDR. Feature matching between raw files was enabled, using a match time window of 2 min. Common contaminants and reverse identifications were filtered out. LFQ intensities calculated when a minimum of 2 peptides were quantified were used for the analysis (Cox *et al.*, 2014).

Mean values of quadruplicate LFQ values were calculated and the enrichment of proteins in samples from *Casp1<sup>mit/mit</sup>* mice over samples from *Casp1<sup>-/-</sup>* or *Nlrp3<sup>-/-</sup>* mice evaluated. Invers relative standard deviation (mean / SD) of *Casp1<sup>mit/mit</sup>* samples was used as an indicator for the specificity of detected proteins.

## SUPPLEMENTAL REFERENCES

- Broz, P., Ruby, T., Belhocine, K., Bouley, D.M., Kayagaki, N., Dixit, V.M., and Monack, D.M. (2012). Caspase-11 increases susceptibility to *Salmonella* infection in the absence of caspase-1. *Nature* *490*, 288–291.
- Cox, J., and Mann, M. (2008). MaxQuant enables high peptide identification rates, individualized p.p.b.-range mass accuracies and proteome-wide protein quantification. *Nature Biotechnology* *26*, 1367–1372.
- Cox, J., Hein, M.Y., Luber, C.A., Paron, I., Nagaraj, N., and Mann, M. (2014). Accurate proteome-wide label-free quantification by delayed normalization and maximal peptide ratio extraction, termed MaxLFQ. *Mol. Cell Proteomics* *13*, 2513–2526.
- Cox, J., Neuhauser, N., Michalski, A., Scheltema, R.A., Olsen, J.V., and Mann, M. (2011). Andromeda: a peptide search engine integrated into the MaxQuant environment. *J. Proteome Res.* *10*, 1794–1805.
- Dick, M.S., Sborgi, L., Rühl, S., Hiller, S., and Broz, P. (2016). ASC filament formation serves as a signal amplification mechanism for inflammasomes. *Nature Communications* *7*, 11929.
- Fernandes-Alnemri, T., Wu, J., Yu, J.-W., Datta, P., Miller, B., Jankowski, W., Rosenberg, S., Zhang, J., and Alnemri, E.S. (2007). The pyroptosome: a supramolecular assembly of ASC dimers mediating inflammatory cell death via caspase-1 activation. *Cell Death Differ* *14*, 1590–1604.
- Gewies, A., Gorka, O., Bergmann, H., Pechloff, K., Petermann, F., Jeltsch, K.M., Rudelius, M., Kriegsmann, M., Weichert, W., Horsch, M., et al. (2014). Uncoupling Malt1 Threshold Function from Paracaspase Activity Results in Destructive Autoimmune Inflammation. *CellReports* *9*, 1292–1305.
- Groß, C.J., Mishra, R., Schneider, K.S., Médard, G., Wettmarshausen, J., Dittlein, D.C., Shi, H., Gorka, O., Koenig, P.-A., Fromm, S., et al. (2016). K<sup>+</sup> Efflux-Independent NLRP3 Inflammasome Activation by Small Molecules Targeting Mitochondria. *Immunity* *1–31*.
- Groß, O., Yazdi, A.S., Thomas, C.J., Masin, M., Heinz, L.X., Guarda, G., Quadroni, M., Drexler, S.K., and Tschopp, J. (2012). Inflammasome activators induce interleukin-1 $\alpha$  secretion via distinct pathways with differential requirement for the protease function of caspase-1. *Immunity* *36*, 388–400.
- Hahne, H., Pachi, F., Ruprecht, B., Maier, S.K., Klaeger, S., Helm, D., Médard, G., Wilm, M., Lemeer, S., and Kuster, B. (2013). DMSO enhances electrospray response, boosting sensitivity of proteomic experiments. *Nature Methods* *10*, 989–991.
- Hermann, M., Cermak, T., Voytas, D.F., and Pelczar, P. (2014). Mouse genome engineering using designer nucleases. *J Vis Exp*.
- Kayagaki, N., Stowe, I.B., Lee, B.L., O'Rourke, K., Anderson, K., Warming, S., Cuellar, T., Haley, B., Roose-Girma, M., Phung, Q.T., et al. (2015). Caspase-11 cleaves gasdermin D for non-canonical inflammasome signaling. *Nature* *1–18*.
- Schneider, K.S., Thomas, C.J., and Groß, O. (2013). Inflammasome Activation and Inhibition in Primary Murine Bone Marrow-Derived Cells, and Assays for IL-1 $\alpha$ , IL-1 $\beta$ , and Caspase-1. In *Methods in Molecular Biology*, (Totowa, NJ: Humana Press), pp. 117–135.